Air-water CO_2 evasion from U.S. East Coast estuaries

Laruelle, Goulven Gildas[1*], Goossens, Nicolas[1], Arndt, Sandra[2], Cai, Wei-Jun[3] & Regnier, Pierre[1]

1 Department Geosciences, Environment and Society, Université Libre de Bruxelles, Brussels, Belgium
2 School of Geographical Sciences, University of Bristol, Bristol, UK
3 School of Marine Science and Policy, University of Delaware, Newark, Delaware, USA

*corresponding author: goulven.gildas.laruelle@ulb.ac.be

Abstract:

This study presents the first regional-scale assessment of estuarine CO_2 evasion along the East coast of the US (25 – 45 °N). The focus is on 42 tidal estuaries, which together drain a catchment of 697000 km^2 or 76 % of the total area within this latitudinal band. The approach is based on the Carbon – Generic Estuarine Model (C-GEM) that allows simulating hydrodynamics, transport and biogeochemistry for a wide range of estuarine systems using readily available geometric parameters and global databases of seasonal climatic, hydraulic, and riverine biogeochemical information. Our simulations, performed using conditions representative of the year 2000, suggest that, together, US East coast estuaries emit 1.9 TgC yr^{-1} in the form of CO_2, which correspond to about 40 % of the carbon inputs from rivers, marshes and mangroves. Carbon removal within estuaries results from a combination of physical (outgassing of supersaturated riverine waters) and biogeochemical processes (net heterotrophy and nitrification). The CO_2 evasion and its underlying drivers show important variations across individual systems, but reveal a clear latitudinal pattern characterized by a decrease in the relative importance of physical over biogeochemical processes along a North-South gradient. Finally, the results reveal that the ratio of estuarine surface area to the river discharge, S/Q (which has a scale of per meter discharged water per year), could be used as a predictor of the estuarine carbon processing in future regional and global scale assessments.

1 Introduction

Carbon fluxes along the land-ocean aquatic continuum are currently receiving increasing attention because of their recently recognized role in the global carbon cycle and anthropogenic CO_2 budget (Bauer et al., 2013; Regnier et al., 2013a; LeQuéré et al., 2014, 2015). Estuaries are important reactive conduits along this continuum, which links the terrestrial and marine global carbon cycles (Cai, 2011). Large amounts of terrestrial carbon transit through these systems, where they mix with carbon from autochthonous, as well as marine sources. During estuarine transit, heterotrophic processes degrade a fraction of the allochthonous and autochthonous organic carbon inputs, supporting a potentially significant, yet poorly quantified CO_2 evasion flux to the atmosphere. Recent estimates suggest that 0.15-0.25 PgC yr^{-1} is emitted from estuarine systems worldwide (Borges and Abril, 2012; Cai, 2011; Laruelle et al., 2010; Regnier et al., 2013a; Laruelle et al., 2013, Bauer et al., 2013). Thus, in absolute terms the global estuarine CO_2 evasion corresponds to about 15% of the open ocean CO_2 uptake despite the much smaller total surface area.

Currently, estimates of regional and global estuarine CO_2 emissions are mainly derived on the basis of data-driven approaches that rely on the extrapolation of a small number of local measurements (Cai, 2011; Chen et al., 2013; Laruelle et al., 2013). These approaches fail to capture the spatial and temporal heterogeneity of the estuarine environment (Bauer et al., 2013) and are biased towards anthropogenically influenced estuarine systems located in industrialized countries (Regnier et al., 2013a). Even in the best surveyed regions of the world (e.g. Australia, Western Europe, North America or China) observations are merely available for a small number of estuarine systems. In addition, if available, data sets are generally of low spatial and temporal resolution. As a consequence, data-driven approaches can only provide first-order estimates of regional and global estuarine CO_2 emissions.

Integrated model-data approaches can help here, as models provide the means to extrapolate over temporal and spatial scales and allow disentangling the complex and very dynamic network of

physical and biogeochemical processes that controls estuarine CO_2 emissions. Over the past decades, increasingly complex process-based models have been applied, in combination with local data, to elucidate the coupled carbon-nutrient cycles on the scale of individual estuaries (e.g., O'Kane, 1980; Soetaert and Herman, 1995; Vanderborght et al., 2002; Lin et al., 2007; Arndt et al., 2009; Cerco et al., 2010; Baklouti et al., 2011). However, the application of such model approaches remains limited to the local scale due to their high data requirements for calibration and validation (e.g. bathymetric and geometric information and boundary conditions), as well as the high computational demand associated with resolving the complex interplay of physical and biogeochemical processes on the relevant temporal and spatial scales (Regnier et al., 2013b). Complex process-based models are thus not suitable for the application on a regional or global scale and, as a consequence, the estuarine carbon filter is, despite its increasingly recognized role in regional and global carbon cycling (e.g. Bauer et al., 2013), typically not taken into account in model-derived regional or global carbon budgets (Bauer et al., 2013). The lack of regional and global model approaches that could be used as stand-alone applications or that could be coupled to regional terrestrial river network models (e.g. GLOBALNEWS: Seitzinger et al., 2005; Mayorga et al., 2010; SPARROW: Schwarz et al., 2006) and continental shelf models (e.g. Hofmann et al., 2011) is thus critical.

The Carbon-Generic Estuary Model (C-GEM (v1.0); Volta et al., 2014) has been developed with the aim of providing such a regional/global modeling tool that can help improve existing, observationally derived first order estimates of estuarine CO_2 emissions. C-GEM (v1.0) has been specifically designed to reduce data requirements and computational demand and, thus, tackles the main impediments for the application of estuarine models on a regional or global scale. The approach takes advantage of the mutual dependency between estuarine geometry and hydrodynamics in alluvial estuaries and uses an idealized representation of the estuarine geometry to support the hydrodynamic calculations. It thus allows running steady state or fully transient annual to multi-decadal simulations for a large number of estuarine systems, using geometric information readily available through maps

or remote sensing images. Although the development of such a regional/global tool inevitably requires simplification, careful model evaluations have shown that, despite the geometric simplification, C-GEM provides an accurate description of the hydrodynamics, transport and biogeochemistry in tidal estuaries (Volta et al., 2014). In addition, the model approach was successfully used to quantify the contribution of different biogeochemical processes for CO_2 air-water fluxes in an idealized, funnel-shaped estuary forced by typical summer conditions characterizing a temperate Western European climate (Regnier et al., 2013b). Volta et al. (2016b) further investigated the effect of estuarine geometry on the CO_2 outgassing using three idealized systems and subsequently established the first regional carbon budget for estuaries surrounding the North Sea by explicitly simulating the six largest systems of the area (Volta et al., 2016a), including the Scheldt and the Elbe for which detailed validation was performed.

Here, we extend the domain of application of C-GEM (v1.0) to quantify CO_2 exchange fluxes, as well as the overall organic and inorganic carbon budgets for the full suite of estuarine systems located along the entire East coast of the United States, one of the most intensively monitored regions in the world. A unique set of regional data, including partial pressure of CO_2 in riverine and continental shelf waters (pCO_2; Signorini et al., 2013; Laruelle et al., 2015), riverine biogeochemical characteristics (Lauerwald et al., 2013), estuarine eutrophication status (Bricker et al., 2007) and estuarine morphology (NOAA, 1985) are available. These comprehensive data sets are complemented by local observations of carbon cycling and CO_2 fluxes in selected, individual estuarine systems (see Laruelle et al., 2013 for a review), making the East coast of the United States an ideal region for a first, fully explicit regional evaluation of CO_2 evasion resolving every major tidal estuary along the selected coastal segment. The scale addressed in the present study is unprecedented so far (> 3000 km of coastline) and covers a wide range of estuarine morphological features, climatic conditions, land-use and land cover types, as well as urbanization levels. The presented study will not only allow a further evaluation of C-GEM (v1.0), but will also provide the first regional-scale assessment of estuarine CO_2 evasion along the East coast of the US (25 – 45 °N)

and will help explore general relationships between carbon cycling and CO_2 evasion, and readily available estuarine geometrical parameters.

After a description of the model itself and of the dataset used to set up the simulations, a local validation is presented which includes salinity, pCO_2 and pH longitudinal profiles for two well monitored systems (the Delaware Bay and the Altamaha River Estuary). The yearly averaged rates of CO_2 exchange at the air-water interface simulated by the model for 13 individual estuaries are also compared with observed values reported in the literature. Next, regional scale simulations for 42 tidal estuaries of the eastern US coast provide seasonal and yearly integrated estimates of the Net Ecosystem Metabolism (NEM), CO_2 evasion and carbon filtering capacity, CFilt. Model results are then used to elucidate the estuarine biogeochemical behavior along the latitudinal transect encompassed by the present study (30-45° N). Finally, our results are used to derive general relationships between carbon cycling and CO_2 evasion, and readily available estuarine geometrical parameters.

2. Regional description and model approach

2.1 Observation-based carbon budget for the East coast of the United States

The study area covers the Atlantic coast of the United States (Fig.1), from the southern tip of Florida (25°N) to Cobscook Bay (45°N) at the US-Canada boundary. This area encompasses distinct climatic zones and land cover types and exhibits a variety of morphologic features (Fig. 1). The region can be subdivided into several sub-regions following a latitudinal gradient (Signorini et al., 2013). In this study, we define three sub-regions following the boundaries suggested by the COSCAT segmentation (Meybeck et al., 2006; Laruelle et al., 2013) and the further subdivision described in Laruelle et al. (2015). From North to South, the regions are called North Atlantic, Mid Atlantic and South Atlantic Regions (Fig. 1). Total carbon inputs from watersheds to US East coast estuaries (Tab. 1) have been

estimated to range from 4.0 to 10.7 Tg C yr^{-1} (Mayorga et al., 2010; Shih et al., 2010; Stets and Strieg, 2012; Tian et al., 2010; Tian et al., 2012), consisting of dissolved organic carbon (DOC; ~50%), dissolved inorganic carbon (DIC; ~40%) and particulate organic carbon (POC; ~10%). In addition, a statistical approach has been applied to estuaries of the region to quantify organic carbon budgets and Net Ecosystem Productivity (NEP) using empirical models (Herrmann et al., 2015).

Recent studies estimated that, along the East coast of the United States, rivers emit 11.4 TgC yr^{-1} of CO_2 to the atmosphere (Raymond et al., 2013), while continental shelf waters absorb between 3.4 and 5.4 TgC yr^{-1} of CO_2 from the atmosphere (Signorini et al., 2013). A total of thirteen local, annual mean estuarine CO_2 flux estimates across the air-water interface based on measurements are also reported in the literature and are grouped along a latitudinal gradient (Tab. 2). Four of these estimates are located in the South Atlantic region (SAR): Sapelo Sound, Doboy Sound, Altamaha Sound (Jiang et al., 2008), and the Satilla River estuary (Cai and Wang, 1998). Three studies investigate CO_2 fluxes in the mid-Atlantic Region (MAR): the York River Estuary (Raymond et al., 2000) and the Hudson River (Raymond et al., 1997). There is also a comprehensive CO_2 flux study for the Delaware Estuary published after the completion of this work (Joeseof et al., 2015). Six systems are located in the North Atlantic region (NAR): The Great Bay, the Little Bay, the Oyster estuary, the Bellamy estuary, the Cocheco estuary (Hunt et al., 2010; 2011), and the Parker River estuary (Raymond and Hopkinson, 2003). The mean annual flux per unit area from these local studies is 11.7±13.1 mol C m^{-2} yr^{-1} and its extrapolation to the total estuarine surface leads to a regional CO_2 evasion estimate of 3.8 Tg C y^{-1}. This estimate is in line with that of Laruelle et al. (2013) for the same region which proposes an average CO_2 emission rate of 10.8 mol C m^{-2} yr^{-1}. Thus, CO_2 outgassing could remove 35% to 95% of the riverine carbon loads during estuarine transit. About 75 % of the air-water exchange occurs in tidal estuaries (2.8 Tg C y^{-1}) while lagoons and small deltas contribute to the remaining 25 %. Although these simple extrapolations from limited observational data are associated with large uncertainties, they highlight the potentially significant contribution of estuaries to the CO_2 outgassing in the region. However, process-based quantifications of regional organic and

inorganic C budgets including air-water CO_2 fluxes for the estuarine systems along the East coast are not available.

2.2 Selection of estuaries

The National Estuarine Eutrophication Assessment (NEAA) survey (Bricker et al., 2007), which uses geospatial data from the National Oceanic and Atmospheric Administration (NOAA) Coastal Assessment Framework (CAF) (NOAA, 1985), was used to identify and characterize 58 estuarine systems discharging along the Atlantic coast of the United States. From this set, 42 'tidal' estuaries, defined as a river stretch of water that is tidally influenced (Dürr et al., 2011), were retained (Fig. 1) to be simulated by the C-GEM model, which is designed to represent such systems. Using outputs from terrestrial models (Hartmann et al., 2009; Mayorga et al., 2010), the cumulated riverine carbon loads for all the non-tidal estuaries that are excluded from the present study amount to 0.9 Tg C yr^{-1} , which represents less than 15% of the total riverine carbon loads of the region. These 16 systems are located in the SAR (10) and in the MAR (6).

The northeastern part of the domain (NAR, Fig. 1; Tab. 1) includes 11 estuaries along the Gulf of Maine and the Scotian shelf, covering a cumulative surface area of 558 km^2. It includes drowned valleys, rocky shores and a few tidal marshes. The climate is relatively cold (annual mean= 8°C) and the human influence is relatively limited because of low population density and low freshwater inputs. The mean estuarine water depth is 12.9 m and the mean tidal range is 2.8 m.

The central zone (MAR) includes 18 tidal estuaries accounting for a total surface area of 9298 km^2. The Chesapeake Bay and the Delaware estuaries alone contribute more than 60% to the surface area of the region. In this region, estuaries are drowned valleys with comparatively high river discharge and intense exchange with the ocean. Several coastal lagoons, characterized by a limited exchange with the ocean are located here, but are not included in our analysis. The Mid-Atlantic Region (MAR) is characterized by a mean annual temperature of 13°C and is strongly impacted by human activities,

due to the presence of several large cities (e.g. New York, Washington, Philadelphia, Baltimore) and intense agriculture. The mean water depth is about 4.7 m and the tidal range is 0.8 m.

The southern Atlantic region (SAR) includes 13 tidal estuaries covering a total surface area of 959 km². These systems are generally dendritic and surrounded by extensive salt marshes. The climate is subtropical with an average annual temperature of 19°C. Land use includes agriculture and industry, but the population density is generally low. Estuarine systems in the SAR are characterized by a shallow mean water depth of 2.9 m and a tidal range of 1.2 m.

2.3 Model set-up

The generic 1D Reactive-Transport Model (RTM) C-GEM (Volta et al., 2014) is used to quantify the estuarine carbon cycling in the 42 systems considered in this study. The approach is based on idealized geometries (Savenije, 2005; Volta et al., 2014) and is designed for regional and global scale applications (Regnier et al., 2013b; Volta et al., 2014, 2016a). The model approach builds on the premise that hydrodynamics exerts a first-order control on estuarine biogeochemistry (Arndt et al., 2007; Friedrichs and Hofmann, 2001) and CO_2 fluxes (Regnier et al., 2013a). The method takes advantage of the mutual dependence between geometry and hydrodynamics in tidal estuaries (Savenije, 1992) and the fact that, as a consequence, transport and mixing can be easily quantified from readily available geometric data (Regnier et al., 2013a; Savenije, 2005; Volta et al., 2016b).

2.3.1 Description of idealized geometries for tidally-averaged conditions

Although tidal estuaries display a wide variety of shapes, they nevertheless share common geometric characteristics that are compatible with an idealized representation (Fig. 2, Savenije, 1986; Savenije, 2005). For tidally-averaged conditions, their width B (or cross-sectional area A) can be described by an exponential decrease as a function of distance, *x*, from the mouth (Savenije, 1986; Savenije, 2005):

$$B = B0 * \exp\left(-\frac{x}{b}\right) \quad (1)$$

where B (m) is the tidally averaged width, B0 (m) the width at the mouth, x (m) the distance from the mouth (x=0) and b (m) the width convergence length (Fig. 2). The width convergence length, b, is defined as the distance between the mouth and the point at which the width is reduced to B0 e^{-1}. It is directly related to the dominant hydrodynamic forcing. A high river discharge typically results in a prismatic channel with long convergence length (river dominated estuary), while a large tidal range results in a funnel-shaped estuary with short convergence length (marine dominated estuary). At the upstream boundary, the estuarine width is given by:

$$B_L = B0 * \exp\left(-\frac{L}{b}\right) \quad (2)$$

Where L denotes the total estuarine length (m) along the estuarine longitudinal axis.

The total estuarine surface S (m^2) can be estimated by integrating equation (1) over the estuarine length:

$$S = \int_0^L B\, dx = b * B0 * \left(1 - \exp\left(-\frac{L}{b}\right)\right) \quad (3)$$

The width convergence length is then calculated from B0, B_L, L and the real estuarine surface area (SR) by inserting equation (2) in equation (3):

$$b = \frac{SR}{B0 - BL} \quad (4)$$

SR is calculated for each system using the SRTM water body data (Fig. 3a), a geographical dataset encoding high-resolution worldwide coastal outlines in a vector format (NASA/NGA, 2003). While such a database exists for a well monitored region such as the East coast of the US, resorting to using the idealized estuarine surface area (S) is necessary in many other regions. The longitudinal

mean, tidally averaged, depth h (m), is obtained from the National Estuarine Eutrophication Assessment database (Bricker et al., 2007).

Using this idealized representation, the estuarine geometry can be defined by a limited number of parameters: the width at the mouth (B_0), the estuarine length (L), the estuarine width at the upstream limit (B_L) and the mean depth h. These parameters can be easily determined from local maps or Google Earth using Geographic Information Systems (GIS) or obtained from databases (NASA/NGA, 2003).

2.3.2 Hydrodynamics, transport and biogeochemistry

Estuarine hydrodynamics are described by the one-dimensional barotropic, cross-sectionally integrated mass and momentum conservation equations for a channel with arbitrary geometry (Nihoul and Ronday, 1976; Regnier et al., 1998; Regnier and Steefel, 1999):

$$r_s \frac{\partial A}{\partial t} + \frac{\partial Q}{\partial x} = 0 \quad (5)$$

$$\frac{\partial U}{\partial t} + U\frac{\partial U}{\partial x} = -g\frac{\partial \zeta}{\partial x} - g\frac{U|U|}{C_Z^2 H} \quad (6)$$

where:

t	time	[s]
x	distance along the longitudinal axis	[m]
A	cross-section area $A = H \cdot B$	[m^2]
Q	cross-sectional discharge $Q = A \cdot U$	[$m^3\ s^{-1}$]
U	flow velocity Q / A	[$m\ s^{-1}$]
r_s	storage ratio $r_s = B_s / B$	[-]

B_s	storage width	[m]
g	gravitational acceleration	[m s^{-2}]
ξ	elevation	[m]
H	total water depth $H = h + \xi(x,t)$	[m]
C_z	Chézy coefficient	[m$^{1/2}$ s^{-1}]

The coupled partial differential equations (Eqs. (5) and (6)) are solved by specifying the elevation ξ_0(t) at the estuarine mouth and the river discharge Q_r(t) at the upstream limit of the model domain.

The one-dimensional, tidally-resolved, advection-dispersion equation for a constituent of concentration *C(x,t)* in an estuary can be written as (e.g. Pritchard, 1958):

$$\frac{\partial C}{\partial t} + \frac{Q}{A}\frac{\partial C}{\partial x} = \frac{1}{A}\frac{\partial}{\partial x}\left(AD\frac{\partial C}{\partial x}\right) + P \qquad (7)$$

where Q(x,t) and A(x,t) denote the cross-sectional discharge and area, respectively and are provided by the hydrodynamic model (eq. 5 and 6). P(x,t) is the sum of all production and consumption process rates affection the concentration of the constituent. The effective dispersion coefficient D (m^2 s^{-1}) implicitly accounts for dispersion mechanisms associated to sub-grid scale processes (Fischer, 1976; Regnier et al., 1998). In general, D is maximal near the sea, decreases upstream and becomes virtually zero near the tail of the salt intrusion curve (Preddy, 1954; Kent, 1958; Ippen and Harleman, 1961; Stigter and Siemons, 1967). The effective dispersion at the estuarine mouth can be quantified by the following relation (Savenije, 1986):

$$D_0 = 26 \cdot (h_0)^{1.5} \cdot (N \cdot g)^{0.5} \qquad (8)$$

where h_0 (m) is the tidally-averaged water depth at the estuarine mouth and N is the dimensionless Canter Cremers' estuary number defined as the ratio of the freshwater entering the estuary during a

tidal cycle to the volume of salt water entering the estuary over a tidal cycle (Simmons, 1955).

$$N = \frac{Q_b \cdot T}{P} \quad (9)$$

In this equation, Q_b is the bankfull discharge ($m^3\ s^{-1}$), T is the tidal period (s) and P is the tidal prism (m^3). For each estuary, N can thus be calculated directly from the hydrodynamic model. The variation in *D* along the estuarine gradient can be described by Van der Burgh's equation (Savenije, 1986):

$$\frac{\partial D}{\partial x} = -K \frac{Q_r}{A} \quad (10)$$

where *K* is the dimensionless Van der Burgh's coefficient and the minus sign indicates that *D* increases in downstream direction (Savenije, 2012). The Van der Burgh's coefficient is a shape factor that has values between 0 and 1 (Savenije, 2012), and is a function of estuarine geometry for tidally average conditions. Therefore, each estuarine system has its own characteristic *K* value, which correlates with geometric and hydraulic scales (Savenije, 2005). Based on a regression analysis covering a set of 15 estuaries, it has been proposed to constrain *K* from the estuarine geometry (Savenije, 1992):

$$K = 4.32 \cdot \frac{h_0^{0.36}}{B_0^{0.21} \cdot b^{0.14}} \quad \text{with} \quad 0 < K < 1 \quad (11)$$

Reaction processes *P* considered in C-GEM comprise aerobic degradation, denitrification, nitrification, primary production, phytoplankton mortality and air-water gas exchange for O_2 and CO_2 (Fig. 4 and Tab. 3). These processes and their mathematical formulation are described in detail in Volta et al. (2014) and Volta et al. (2016a).

The non-linear partial differential equations for the hydrodynamics are solved by a finite difference scheme following the approach of (Regnier et al., 1997; Regnier and Steefel, 1999) and (Vanderborght et al., 2002). The timestep Δt is 150s and the grid size Δx is constant along the

longitudinal axis of the estuary. The grid size default value is 2000 m, but can be smaller for short length estuaries to guarantee a minimum of 20 grid points within the computational domain. Transport and reaction terms are solved in sequence within a single timestep using an operator splitting approach (Regnier et al., 1997). The advection term in the transport equation is integrated using a third-order accurate total variation diminishing (TVD) algorithm with flux limiters (Regnier et al., 1998), ensuring monotonicity (Leonard, 1984), while a semi-implicit Crank-Nicholson algorithm is used for the dispersion term (Press et al., 1992). These schemes have been extensively tested using the CONTRASTE estuarine model (e.g. Regnier et al., 1998; Regnier and Steefel, 1999; Vanderborght et al., 2002) and guarantee mass conservation to within <1%. The reaction network (including erosion-deposition terms when the constituent is a solid species), is numerically integrated using the Euler method (Press et al., 1992). The primary production dynamics, which takes into account the combined effects of nutrients limitation and light attenuation in the water column induced by its background turbidity and SPM concentration, requires vertical resolution of the photic depth. The latter is calculated according to the method described in Vanderborght et al. (2007). This method assumes an exponential decrease of the light in the water column (Platt et al., 1980), which is solved using a Gamma function.

2.4 Boundary and forcing conditions

Boundary and forcing conditions are extracted from global databases and global model outputs that are available at 0.5° resolution. Therefore, C-GEM simulations are performed at the same resolution according to the following procedure. First, 42 coastal cells corresponding to tidal estuaries are identified in the studied area (Fig. 1). If the mouth of an estuary is spread over several 0.5° grid cells, those cells are regrouped in order to represent a single estuary (e.g. Delaware estuary), and subsequently, a single idealized geometry is defined as described above. The model outputs (Hartmann et al. , 2009; Mayorga et al., 2010) and databases (Antonov et al., 2010; Garcia et al.,

2010a; Garcia et al., 2010b) used to constrain our boundary conditions are representative of the year 2000.

For each resulting cell, boundary and forcing conditions are calculated for the following periods: January-March; April-June; July-September and October-December. This allows for an explicit representation of the seasonal variability in the simulations.

2.4.1 External forcings

Transient physical forcings are calculated for each season and grid cell using monthly mean values of water temperature (World Ocean Atlas: Antonov et al. 2010; Locarini et al., 2010) and seasonal averaged values for wind speed (Cross-Calibrated-Multi-Platform (CCMP) Ocean Surface Wind Vector Analyses project (Atlas et al., 2011)). Mean daily solar radiation and photoperiods (corrected for cloud coverage using the ISCCP Cloud Data Products, Rossow and Schiffer, 1999) are calculated depending on latitude and day of the year using a simple model (Brock, 1981).

2.4.2 Riverine discharge, concentrations and fluxes

River discharges are extracted from the UNH/GRDC runoff dataset (Fekete et al., 2002). These discharges represent long-term averages (1960-1990) of monthly and annual runoff at 0.5 degree resolution. The dataset is a composite of long-term gauging data, which provides average runoff for the largest river basins, and a climate driven water balance model (Fekete et al., 2002). Total runoff values are then aggregated for each watershed at the coarser 0.5 degree resolution (Fig. 3b). Next, seasonal mean values (in $m^3 s^{-1}$) are derived in order to account for the intra-annual variability in water fluxes. Based on annual carbon and nutrients inputs from the watersheds (Mg y^{-1}), mean annual concentrations (mmol m^{-3}) are estimated for each watershed using the UNH/GRDC annual runoff ($km^3 y^{-1}$). Mean seasonal concentrations are then calculated from the seasonally resolved river water fluxes of a given sub-region.

330 Annual inputs of dissolved organic carbon (DOC), particulate organic carbon (POC) and inorganic
331 nutrients are derived from the globalNEWS2 model (Mayorga et al., 2010). Global NEWS is a spatially
332 explicit, multi-element (N, P, Si, C) and multi-form global model of nutrient exports by rivers. In a
333 nutshell, DOC exports are a function of runoff, wetland area, and consumptive water use (Harrison
334 et al., 2005). No distinction is made between agricultural and natural landscapes, since they appear
335 to have similar DOC export coefficients (Harrison et al., 2005). Sewage inputs of OC are ignored in
336 GlobalNEWS, because their inclusion did not improve model fit to data (Harrison et al., 2005). POC
337 exports from watersheds are estimated using an empirical relationship with Suspended Particulate
338 Matter (SPM; Ludwig et al., 1996). Inorganic nitrogen (DIN) and phosphorus (DIP) fluxes calculated
339 by GlobalNEWS depend on agriculture and tropical forest coverage, fertilizer application, animal
340 grazing, sewage input, atmospheric N deposition and biological N fixation (Mayorga et al., 2010). The
341 inputs of dissolved silica (DSi) are controlled by soil bulk density, precipitation, slope, and presence
342 of volcanic lithology (Beusen et al., 2009).

343 The DIN speciation is not provided by the GlobalNEWS2 model. The NH_4 and NO_3 concentrations are
344 therefore determined independently on the basis of an empirical relationship between ammonium
345 fraction (NH4/DIN ratio) and DIN loads (Meybeck, 1982). Dissolved Oxygen (DO) concentrations are
346 extracted from the water quality criteria recommendations published by the United States
347 Environmental Protection Agency (EPA, 2009). The same source is used for phytoplankton
348 concentrations, using a chlorophyll-a to phytoplankton carbon ratio of 50 gC $(gChla)^{-1}$ (Riemann et
349 al., 1989) to convert the EPA values to carbon units used in the present study.

350 Inputs of dissolved inorganic carbon (DIC) and total Alkalinity (ALK) are calculated from values
351 reported in the GLORICH database (Hartmann et al., 2009). For each watershed, seasonal mean
352 values of DIC and ALK concentrations are estimated from measurements performed at the sampling
353 locations that are closest to the river-estuary boundary. The spatial distribution of annual inputs of
354 TOC=DOC+POC, DIC, and TC=TOC+DIC from continental watersheds to estuaries are reported in Fig.

355 5a, 5c and 5d, respectively. The contribution of tidal wetlands to the TOC inputs is also shown (Fig.
356 5b). Overall, the TC input over the entire model domain is estimated at 4.6 Tg C yr^{-1}, which falls in
357 the lower end of previous reported estimations (Najjar et al. 2012).

358

359 **2.4.3 Inputs from tidal wetlands**

360 The DOC input of estuarine wetlands (Fig. 5b) scales to their fraction, W, of the total estuarine and is
361 calculated using the GlobalNEWS parameterization:

$$Y\_DOC = \frac{\left[(E\_C_{wet} * W) + E\_C_{dry} * (1 - W)\right] * R^{a} * Q_{act}}{Q_{nat}} \quad (12)$$

362

$$\frac{Y\_DOC_{wet}}{Y\_DOC} = \frac{E\_C_{wet} * W}{E\_C_{wet} * W + E\_C_{dry} * (1 - W)} \quad (13)$$

363

364 where Y_DOC is the DOC yield (kg C km^{-2} y^{-1}) calculated for the entire watershed, Y_DOC_{wet} is the
365 estimated DOC yield from wetland areas (kg C km^{-2} y^{-1}), Q_{act}/Q_{nat} is the ratio between the measured
366 discharge after dam construction and before dam construction, E_C_{wet} and E_C_{dry} (kg C km^{-2} y^{-1}) are
367 the export coefficients of DOC from wetland and non-wetland soils, respectively. W is the
368 percentage of the land area within a watershed that is covered by wetlands, R is the runoff (m y^{-1})
369 and *a* is a unit-less calibration coefficient defining how non-point source DOC export responds to
370 runoff. The value of a is set to 0.95, consistent with the original GlobalNEWS -DOC model of Harrison
371 et al. (2005). The carbon load Y_DOC_{wet} is then exported as a diffuse source along the relevant
372 portions of estuary. The estuarine segments receiving carbon inputs from tidal wetlands are
373 identified using the National Wetlands Inventory of the U.S. Fish and Wildlife Service (U.S. Fish and
374 Wildlife Service, 2014). The inputs from those systems are then allocated to the appropriate grid cell

of the model domain using GIS. The flux calculated is an annual average that is subsequently partitioned between the four seasons as a function of the mean seasonal temperature, assumed to be the main control of the wetland-estuarine exchange. This procedure reflects the observation that in spring and early summer, DOC export is small as a result of its accumulation in the salt marshes induced by the high productivity (Dai and Wiegert, 1996), (Jiang et al., 2008). In late summer and fall, the higher water temperature and greater availability of labile DOC contribute to higher bacterial remineralization rates in the intertidal marshes (Cai et al., 1999; Middelburg et al., 1996; Wang and Cai, 2004), which induce an important export. This marsh production-recycle-export pattern is consistent with the observed excess DIC signal in the offshore water (Jiang et al. 2013). DIC export from tidal wetlands is neglected here because it is assumed that OC is not degraded before reaching the estuarine realm. Although this assumption may lead to an overestimation of OC export from marshes and respiration in estuarine water, it will not significantly affect the water pCO_2 and degassing in the estuarine waters because mixing is faster than respiration.

2.4.4 Concentrations at the estuarine mouth

For each estuary, the downstream boundary is located 20 km beyond the mouth to minimize the bias introduced by the choice of a fixed concentration boundary condition to characterize the ocean water masses (e.g. Regnier et al., 1998). This approach also reduces the influence of marine boundary conditions on the simulated estuarine dynamics, especially for all organic carbon species whose concentrations are fixed at zero at the marine boundary. This assumption ignores the intrusion of marine organic carbon into the estuary during the tidal cycle but allows focusing on the fate of terrigenous material and its transit through the estuarine filter. DIC concentrations are extracted from the GLODAP dataset (Key et al., 2004), from which ALK and pH are calculated assuming CO_2 equilibrium between coastal waters and the atmosphere. The equilibrium value is computed using temperature (WOA2009, Locarnini et al., 2010) and salinity (WOA2009, Antonov et al. (2010)) data which vary both spatially and temporally. The equilibrium approach is a reasonable

assumption because differences in partial pressure ΔpCO_2 between coastal waters and the atmosphere are generally much smaller (0-250 µatm (Signorini et al., 2013)) than those reported for estuaries (ΔpCO_2 in the range 0-10000 µatm (Borges and Abril, 2012)). Salinity, DO, NO_3, DIP and DSi concentrations are derived from the World Ocean Atlas (Antonov et al., 2010; Garcia et al., 2010a; Garcia et al., 2010b). NH_4 concentrations are set to zero in marine waters. For all variables, seasonal means are calculated for each grid cell of the boundary.

2.5 Biogeochemical indicators

The model outputs (longitudinal profiles of concentration and reaction rates) are integrated in time over the entire volume or surface of each estuary to produce the following indicators of the estuarine biogeochemical functioning (Regnier et al., 2013b): the mean annual Net Ecosystem Metabolism (*NEM*), the air-water CO_2 flux (FCO_2), the carbon and nitrogen filtering capacity (*CFilt* and *NFilt*) and their corresponding element budgets. The *NEM* (molC y^{-1}) (Caffrey, 2004; Odum, 1956) is defined as the difference between net primary production (*NPP*) and total heterotrophic respiration (*HR*) at the system scale:

$$NEM = \int_0^{365} \int_0^{L} [NPP(x,t) - R_{aer}(x,t) - R_{den}(x,t)] * B(x) * H(x,t)\, dx\, dt \quad (14)$$

where *NPP* is the Net Primary Production (mol C m^{-3} y^{-1}), R_{aer} the aerobic degradation of organic matter (in mol C m^{-3} y^{-1}) and R_{den} the denitrification (in mol C m^{-3} y^{-1}) (see Volta et al., 2014 for detailed formulations). *NEM* is thus controlled by the production and decomposition of autochthonous organic matter, by the amount and degradability of organic carbon delivered by rivers and tidal wetlands and by the export of terrestrial and in-situ produced organic matter to the adjacent coastal zone. Following the definition of *NEM*, the trophic status of estuaries can be net

heterotrophic (NEM<0) when *HR* exceeds *NPP* or net autotrophic (NEM>0), when *NPP* is larger than *HR* because the burial and export of autochthonous organic matter exceeds the decomposition of river-borne material.

The FCO_2 (mol C y^{-1}) is defined as:

$$FCO_2 = \int_0^{365} \int_0^{L} RCO_2(x,t) * B(x)\, dx\, dt \quad (15)$$

$$RCO_2(x,t) = -\mathrm{v_p}(\mathrm{x,t})\left(\left[CO_{2(aq)}\right](x,t) - K_0(x,t) * P_{CO2}(x,t)\right) \quad (16)$$

where RCO_2 (molC m^{-2} y^{-1}) is the rate of exchange in CO_2 at the air-water interface per unit surface area, v_p is the piston velocity (m y^{-1}) and is calculated according to Regnier et al. (2002) to account for the effect of current velocity and wind speed, [*CO2(aq)*] is the concentration of CO_2 in the estuary (mol m^{-3}), K_0 is Henry's constant of CO_2 in sea water (mol m^{-3} atm^{-1}) and P_{CO2} is the atmospheric partial pressure in CO_2 (atm).

The carbon filtering capacity (in %) corresponds to the fraction of the river-borne supply that is lost to the atmosphere and is defined here as the ratio of the net outgassing flux of CO_2 and the total inputs of C, e.g. total carbon expressed as the sum of inorganic and organic carbon species, both in the dissolved and particulate phases.

$$CFilt = \frac{FCO_2}{\int_0^{365} Q * [TC]_{riv}\, dt} * 100 \quad (17)$$

where $[TC]_{riv}$ denote the total concentrations of C in the riverine inputs.

Fluxes per unit area for FCO_2 and *NEM*, noted $\overline{FCO_2}$ and $\overline{NEM}$, respectively, are defined in mol C m^{-2} y^{-1} and are calculated by dividing the integrated values calculated above by the (idealized) estuarine surface *S*:

$$\overline{NEM} = \frac{NEM}{S} * 1000 \quad (18)$$

$$\overline{FCO_2} = \frac{FCO_2}{S} * 1000 \quad (19)$$

Seasonal values for the biogeochemical indicators are calculated using the same formula as above, but calculate the integral over a seasonal rather than annual timescale (i.e. 3 months).

2.6 Model-data comparison

C-GEM has been specifically designed for an application on a global/regional scale requiring the representation of a large number of individual and often data-poor systems. Maximum model transferability and minimum validation requirements were thus central to the model design process and the ability of the underlying approach in reproducing observed dynamics with minimal calibration effort has been extensively tested. The performance C-GEM's one-dimensional hydrodynamic and transport models using idealized geometries have been evaluated for a number of estuarine systems exhibiting a wide variety of shapes (Savenije, 2012). In particular, it has been shown that the estuarine salt intrusion can be successfully reproduced using the proposed modeling approach (Savenije 2005; Volta et al., 2014; 2016b). In addition, C-GEM's biogeochemistry has also been carefully validated for geometrically contrasting estuarine system in temperate climate zones. Simulations for the Scheldt Estuary (Belgium and the Netherlands), a typical funnel-shaped estuary, were validated through model-data and model-model comparison (Volta et al., 2014; Volta et al., 2016a). Furthermore, simulations for the Elbe estuary (Germany), a typical prismatic shape estuary that drains carbonate terrains and, thus, exhibits very high pH was validated against field data (Volta et al., 2016a). In addition, C-GEM carbon budgets have been compared budget derived from observations for 6 European estuaries discharging in the North Sea (Volta et al., 2016a). Although C-GEM has been specifically designed and tested for the type of regional application presented here, its transferability from North Sea to US East Coast estuaries was further evaluated by assessing its

466 performance in two East Coast estuaries. First, the hydrodynamic and transport model was tested
467 for the Delaware Bay (MAR). The model was forced with the monthly, minimal and maximal
468 observed discharge at Trenton over the period between 1912 and 1985 (UNH/GRDC Database,
469 GRDC, 2014). Simulated salinity profiles are compared with salinity observations from January,
470 February, May and June (the months with the highest number of data entries), which were extracted
471 from the UNH/GRDC Database. Figure 6 shows that the model captures both the salinity intrusion
472 length and the overall shape of the salinity profile well. In addition, the performance of the
473 biogeochemical model and specifically its ability to reproduce pH and pCO_2 profiles was evaluated by
474 a model-data comparison for both the Delaware Bay (MAR) in July 2003 and the Altamaha river
475 estuary (SAR) in October 1995. Similar to Volta et al., 2016a, the test systems were chosen due to
476 their contrasting geometries. The Delaware Bay is a marine dominated system characterized by a
477 pronounced funnel shape, while the Altamaha River has a prismatic estuary characteristic of river
478 dominated systems (Jiang et al., 2008). Monthly upstream boundary conditions for nutrients, as well
479 as observed pH data and calculated pCO_2 are extracted from datasets described in (Sharp, 2010) and
480 (Sharp et al., 2009) for the Delaware and in Cai and Wang (1998), Jiang et al. (2008) and (Cai et al.,
481 1998) for the Altamaha river estuary. The additional forcings and boundary conditions are set
482 similarly to the simulation for 2000 (see Tab. 2, 3, 4, 5, 6 in SI). Figure 7 shows that measured and
483 simulated pH values are in good agreement with observed pH and observation-derived calculations
484 of pCO_2. In the Delaware Bay, a pH minimum is located around km 140 and is mainly caused by
485 intense nitrification sustained by large inputs of NH_4 from the Philadelphia urban area, coupled to an
486 intense heterotrophic activity. Both processes lead to a well-developed pCO_2 increase in this area
487 (Fig. 7c). Overall, the longitudinal pCO_2 profile of the Delaware estuary is characterized by values
488 close to equilibrium with the atmosphere in the widest section of the Delaware Bay (near the
489 estuarine mouth and throughout the 40 first kilometers of the system) and values above 1200 µatm
490 at kilometer 150 and beyond, where characteristic salinities are below 5. Although the profile
491 presented here is simulated using boundary conditions representative of July 2003 and no pCO_2 data

were available for validation for this period, a recent study by Joesoef et al. (2015) reports a similar longitudinal pCO_2 profile in July 2013. For the Altamaha river estuary, pH steadily increases from typical river to typical coastal ocean values (Fig. 7b). In addition, both observations and model results reveal that outgassing is very intense in the low-salinity region with more than a 5 fold decrease in pCO_2 between salinity 0 and 5 (Fig. 7d).

While such local validations allow assessing the performance of the model for a specific set of conditions, the purpose of this study is to capture the average biogeochemical behavior of the estuaries of the eastern coast of the US. Therefore, in addition to the system-specific validation, published annually averaged FCO_2 estimates for 12 tidal systems located within the study area collected over the 1994-2006 period are compared to simulated FCO_2 for conditions representative of the year 2000. Overall, simulated FCO_2 are comparable to values reported in the literature (Tab. 2). Although significant discrepancies are observed at the level of individual systems, the model captures remarkably well the overall behaviors of estuaries along the East coast of the US in term of intensity of CO_2 evasion rate. The model simulates low CO_2 efflux (< 5 mol C m^{-2} yr^{-1}) for the 6 systems were such conditions have been observed, while the 5 systems for which the CO_2 evasion exceeds 10 mol C m^{-2} yr^{-1} are the same in the observations and in the model runs. The discrepancies at the individual system level likely result from a combination of factors, including the choice of model processes and there parametrization, the uncertainties in constraining boundary conditions and the limited representability of instantaneous and local observations.

3 Results and discussion

3.1 Spatial variability of estuarine carbon dynamics

Figure 8 presents the spatial distribution of simulated mean annual $\overline{FCO_2}$ and -$\overline{NEM}$ (Fig. 8a), as well as FCO_2 and -*NEM* (Fig. 8b). In general, mean annual $\overline{FCO_2}$ are about 30% larger than mean annual $\overline{NEM}$, with the exception of six estuaries situated in the North of the coastal segment. Overall, the

$\overline{NEM}$ is characterized by smaller system to system variability compared to the $\overline{FCO_2}$ in all regions. In addition, Fig. 8 reveals distinct differences across the three coastal segments and highlights the important influence of the estuarine geometry and residence time, as well as the latitudinal temperature gradient on estuarine carbon cycling.

Overall, $\overline{FCO_2}$ values are the lowest in the NAR (mean flux = 17.3 ± 16.4 mol C m^{-2} y^{-1}; surface weighted average = 23.1 mol C m^{-2} y^{-1}), consistent with previously reported very low values for small estuaries surrounding the Gulf of Maine (Hunt et al., 2010; 2011; Tab. 2). In contrast, $\overline{NEM}$ reveals a regional minimum in the NAR (-51.2 ± 16.6 mol C m^{-2} y^{-1}; surface weighted average = -52.8 mol C m^{-2} y^{-1}). The MAR is characterized by intermediate values for $\overline{FCO_2}$, with a mean flux of 26.3 ± 34.6 mol C m^{-2} y^{-1} (surface weighted average =11.1 mol C m^{-2} y^{-1}) and lowest values for $\overline{NEM}$ (-15.1 ± 14.2 mol C m^{-2} y^{-1}; surface weighted average =-7.4 mol C m^{-2} y^{-1}). This region also shows the largest variability in CO_2 outgassing compared to the NAR and SAR, with the standard deviation exceeding the mean $\overline{FCO_2}$, and individual estimates ranging from 3.9 mol C m^{-2} y^{-1} to 150.8 mol C m^{-2} y^{-1}. This variability is mainly the result of largely variable estuarine surface areas and volumes. Some of the largest East coast estuaries (e.g. Chesapeake and Delaware Bays), as well as some of smallest estuaries (e.g. York River and Hudson River estuaries, Raymond et al., 1997; 2000), are located in this region (Tab. 2 and 4). The maximum values of 150.8 mol C m^{-2} y^{-1} simulated in the MAR are similar to the highest FCO_2 reported in the literature (132.3 mol C m^{-2} y^{-1} for the Tapti estuary in India; Sarma et al., 2012). The SAR is characterized by the highest mean $\overline{FCO_2}$ (46.7 ± 33.0 mol C m^{-2} y^{-1}; surface weighted average = 40.0 mol C m^{-2} y^{-1}) and intermediate $\overline{NEM}$ (-36.8 ± 24.7 mol C m^{-2} y^{-1}; surface weighted average = -31.2 mol C m^{-2} y^{-1}).

The NAR is characterized by a regional minimum in $\overline{FCO_2}$, and only contributes 4.6% to the total FCO_2 of the East coast of the US, owing to the small cumulative surface area available for gas exchange in its 10 estuarine systems. In contrast, the 18 MAR estuaries, with their large relative contribution to the total regional estuarine surface area, account for as much as 70.1% of the total

outgassing. Because of their smaller cumulated surface area compared to those of the MAR, the 14 SAR estuaries account for merely 25.3% of the total outgassing despite their regional maximal $\overline{FCO_2}$. A similar, yet slightly less pronounced pattern emerges for the $\overline{NEM}$. The NAR, MAR and SAR respectively contribute 13.7%, 60.7% and 25.6% to the total regional net ecosystem metabolism. The comparatively larger relative contribution of the NAR to the total *NEM* as compared to the total FCO_2 can be explained by the importance of the specific aspect ratio for NEM. A larger ratio of estuarine width B0 and convergence length b corresponds to a more funnel shaped estuary while a low ratio corresponds to a more prismatic geometry (Savenije, 2005; Volta et al., 2014). In the NAR, estuaries are generally characterized by relatively narrow widths and deep-water depths, thus limiting the potential surface area for gas exchange with the atmosphere. However, the relative contribution of each region to the total regional *NEM* and FCO_2 is largely controlled by estuarine surface area. Figure 9 illustrates the cumulative *NEM* (a) and FCO_2 (b) as a function of the cumulative estuarine surface areas. The disproportionate contribution of large estuaries from the MAR translates into a handful of systems (Chesapeake and Delaware Bays and the main tributaries of the former, in particular) contributing to roughly half of the regional *NEM* and FCO_2, in spite of relatively low individual rates per unit surface area. However, the smallest systems (mostly located in the NAR and SAR) nevertheless still contribute a significant fraction to the total regional *NEM* and FCO_2. The 27 smallest systems merely account for less than 10% of the total regional estuarine surface area, yet contribute 38% and 29% to the total regional *NEM* and FCO_2, respectively (Fig. 9). This disproportioned contribution can be mainly attributed to their high individual $\overline{FCO_2}$ and $\overline{NEM}$. This is illustrated by the average simulated $\overline{FCO_2}$ for all 27 smallest systems (calculated as the sum of each estuarine CO_2 outgassing per unit surface area divided by the total number of estuarine systems) which is significantly higher (30.2 mol C m^{-2} y^{-1}) than its surface weighted average (14 mol C m^{-2} y^{-1}). Thereby accounting for the disproportionate contribution of very large systems (calculated as the sum of each estuarine CO_2 outgassing divided by the total estuarine surface area across the region).

Following the approach used in Regnier et al. (2013b), the contribution of each biogeochemical process to FCO_2 is assessed by evaluating their individual contribution to DIC and ALK changes taking into account the local buffering capacity of an ionic solution when TA and DIC are changing due to internal processes, but ignoring advection and mixing (Zeebe and Wolf-Gladrow 2001). In the present study, we quantify the effect of the NEM on the CO_2 balance, which is almost exclusively controlled by aerobic degradation rates because the contributions of denitrification and NPP to the net ecosystem balance are small. Nitrification, a process triggered by the transport and/or production of NH_4 in oxygenated waters, favors outgassing through its effect on pH, which shifts the acid-base equilibrium of carbonate species and increases the CO_2 concentration. The contribution of supersaturated riverine waters to the overall estuarine CO_2 dynamics is calculated as difference between all the other processes creating or consuming CO_2.. Figure 10a presents the contribution of the annually integrated *NEM*, nitrification and evasion of supersaturated, DIC enriched riverine waters to the total outgassing for each system, as well as for individual regions of the domain. The calculation of these annual values is based on the sum of the seasonal fluxes. Model results reveal that, regionally, the *NEM* supports about 50% of the estuarine CO_2 outgassing, while nitrification and riverine DIC inputs sustain about 17% and 33% of the CO_2 emissions, respectively. The relative significance of the three processes described above shows important spatial variability. In the NAR, oversaturated riverine waters and NEM respectively sustain 50% and 44% of the outgassing within the sub-region, while nitrification is of minor importance (6%). In the MAR, the contribution of riverine DIC inputs is significantly lower (~30%) and the main contribution to the outgassing is *NEM* (~50%); nitrification accounting for slightly less than 20% of the outgassing. In the SAR, the riverine contribution is even lower (~20%), and the outgassing is mainly attributed to the *NEM* (~55%) and nitrification (~25%). Therefore, although the model results reveal significant variability across individual systems, a clear latitudinal trend in the contribution to the total FCO_2 emerge from the analysis; the importance of oversaturated riverine water decreasing from North to South, while *NEM* and nitrification increase along the same latitudinal gradient. The increasing relative importance of

593 estuarine biogeochemical processes over riverine DIC inputs as drivers of FCO_2 along the North-
594 South gradient is largely driven by increasing temperatures from North to South, especially in the
595 SAR region (Tab. SI 1).

596 Contrasting patterns across the 3 regions can also be observed with respect to carbon filtering
597 capacities, *CFilt* (Fig. 10b). In the NAR, over 90% of the riverine carbon flux is exported to the coastal
598 ocean. However, in the MAR, the high efficiency of the largest systems in processing organic carbon
599 results in a regional *CFilt* that exceeds 50%. This contrast between the NAR and the MAR and its
600 potential implication for the carbon dynamics of the adjacent continental shelf waters has already
601 been discussed by Laruelle et al. (2015). In the NAR, short estuarine residence results in a much
602 lower removal of riverine carbon by degassing compared to the MAR. Laruelle et al. (2015)
603 suggested that this process could contribute to the weaker continental shelf carbon sink adjacent to
604 the NAR, compared to the MAR. In the SAR, most estuaries remove between 40% and 65% of the
605 carbon inputs. The high temperatures observed and resulting accelerated biogeochemical process
606 rates in this region favor the degradation of organic matter and contribute to increase the estuarine
607 filtering capacity for carbon. However, in the SAR, a large fraction of the OC loads is derived from
608 adjacent salt marshes located along the estuarine salinity gradients, thereby reducing the overall
609 residence time of OC within the systems. The filtering capacity of the riverine OC alone, which
610 transits through the entire estuary, would thus be higher than the one calculated here. As a
611 consequence, highest C retention rates are expected in warm tidal estuaries devoid of salt marshes
612 or mangroves (Cai, 2011).

613 **3.2 Seasonal variability of estuarine carbon dynamics**

614 Carbon dynamics in estuaries of the US East coast not only show a marked spatial variability, but also
615 vary on the seasonal timescale. Table 5 presents the seasonal distribution of *NEM* and FCO_2 for each
616 sub-region. In the NAR, a strong seasonality is simulated for the *NEM* and the summer period
617 contributes more than a third to the annually integrated value. The outgassing reveals a lower

seasonal variability and is only slightly higher than summer outgassing during fall and lower during spring. In the MAR, summer contributes more to the *NEM* (>28% of the yearly total) than any other season, but seasonality is less pronounced than in the NAR. Here, FCO_2 is largest in winter and particularly low during summer. In the SAR, summer accounts for 30 % of the NEM, while spring contributes 21 %. FCO_2 is relatively constant throughout the year suggesting that seasonal variations in carbon processing decrease towards the lower latitudes in the SAR. This is partly related to the low variability in river discharge throughout the year in lower latitudes (Tab. SI1). In riverine dominated systems with low residence times, such as, for instance, the Altamaha River estuary, the CO_2 exchange at the air-water interface is mainly controlled by the river discharge because the time required to degrade the entire riverine organic matter flux exceeds the transit time of OC through the estuary. Therefore, the riverine sustained outgassing is highest during the spring peak discharge periods. In contrast, the seasonal variability in FCO_2 in long-residence, marine-dominated systems with large marsh areas (e.g. Sapelo and Doboy Sound) is essentially controlled by seasonal temperature variations. Its maximum is reached during summer when marsh plants are dying and decomposing, as opposed to spring when marshes are in their productive stage (Jiang et al., 2008). These contrasting seasonal trends have already been reported for different estuarine systems in Georgia, such as the Altamaha Sound, the Sapelo Sound and the Doboy Sound (Cai, 2011). At the scale of the entire East coast of the US, the seasonal trends in *NEM* reveal a clear maximum in summer and minimal values during autumn and winter. The seasonality of FCO_2 is much less pronounced because the outgassing of oversaturated riverine waters throughout the year contributes to a large fraction of the FCO_2 and dampens the effect of the temperature dependent processes (*NEM* and denitrification). In our simulations, the competition between temperature and river discharge is the main driver of the seasonal estuarine carbon dynamics is. When discharge increases, the carbon loads increase proportionally and the residence time within the system decreases, consequently limiting an efficient degradation of organic carbon input fluxes. In warm

643 regions like the SAR, the temperature is sufficiently high all year round to sustain high C processing
644 rates and this explains the reduced seasonal variability in NEM.
645
646 **3.3 Regional carbon budget: a comparative analysis**

647 The annual carbon budget for the entire East coast of the US is summarized in Fig. 11a. The total
648 carbon input to estuaries along the East coast of the US is 4.6 Tg C y^{-1}, of which 42% arrives in
649 organic form and 58% in inorganic form**.** Of this total input, saltmarshes contribute 0.6 Tg C yr^{-1},
650 which corresponds to about 14% of the total carbon loads and 32% of the organic loads in the
651 region. The relative contribution of the saltmarshes to the total carbon input increases towards low
652 latitudes and is as high as 60% in the SAR region. Model results suggest that 2.7 Tg C y^{-1} is exported
653 to the continental shelf (25% as TOC and 75% as DIC), while 1.9 Tg C y^{-1} is emitted to the
654 atmosphere. The overall carbon filtering capacity of the region thus equals 41% of the total carbon
655 entering the 42 estuarine systems (river + saltmarshes). Because of the current lack of a benthic
656 module in C-GEM, the water column carbon removal occurs entirely in the form of CO_2 outgassing
657 and does not account for the potential contribution of carbon burial in sediments. The estimated
658 estuarine carbon retention presented here is thus likely a lower bound estimate. Reported to the
659 modeled surface area of the region, the total FCO_2 of 1.9 Tg C y^{-1} translates into a mean air water
660 CO_2 flux of about 14 mol C m^{-2} y^{-1}. This value is slightly higher than the estimate of 10.8 mol C m^{-2} y^{-1}
661 calculated by Laruelle et al., (2013) on the basis of local $\overline{FCO_2}$ estimates assumed to be
662 representative of yearly averaged conditions (see section 2.1). The latter was calculated as the
663 average of 13 annual $\overline{FCO_2}$ values reported in the literature (Tab. 2), irrespective of the size of the
664 systems. This approach is useful and widely used to derive regional and global carbon budgets
665 (Borges et al., 2005; Laruelle et al., 2010; Chen et al., 2013). However, it may lead to potentially
666 significant errors (Volta et al., 2016a) due to the uncertainty introduced by the spatial interpolation

667 of local measurements to large regional surface areas, while useful and widely used to derive
668 regional and global carbon budgets.

669 Regional C budgets are sparse. To our knowledge, the only other published regional assessment of
670 the estuarine carbon and CO_2 dynamics comes from a relatively well studied region: the estuaries
671 flowing into the North Sea in Western Europe (Fig. 11b). This budget was calculated using a similar
672 approach (Volta 2016a) and thus provides an ideal opportunity for a comparative assessment of C
673 cycling in these regions. However, it is important to note that there are also important differences in
674 the applied model approaches and those differences should be taken into account when comparing
675 the derived budgets. In particular, the NW European study is based on a simulation of the 6 largest
676 systems only (Elbe, Scheldt, Thames, Ems, Humber and Weser), accounting for about 40% for the
677 riverine carbon loads of the region. It assumes that the intensity of carbon processing and evasion in
678 all other smaller estuaries discharging into the North Sea (16 % of the carbon loads) can be
679 represented by the average of the 6 largest system simulation results. In addition, the Rhine-Meuse
680 system, which alone accounts for 44% of the carbon riverine inputs of the region, was treated as a
681 passive conduit with respect to carbon due to its very short freshwater residence time (Abril et al.,
682 2002). The contribution of saltmarshes to the regional carbon budget was also ignored because their
683 total surface area is much smaller than along the US East coast (Regnier et al., 2013b). Another
684 important difference is the inclusion of seasonality in the present study while the budget calculated
685 for the North Sea is derived from yearly average conditions (Volta et al., 2016a).

686 Overall, although both regions receive similar amounts of C from rivers (4.6 Tg C y^{-1} and 5.9 Tg C y^{-1}
687 for the East coast of the US and the North Sea, respectively), they reveal significantly different C
688 filtering capacities. While the estuaries of the East coast of the US filter 41% of the riverine TC loads,
689 those from the North Sea only remove 8% of the terrestrial-derived material. This is partly due to the
690 large amounts of carbon transiting through the 'passive' Rhine-Meuse system. The regional filtering
691 capacity is higher (15%) when this system is excluded from the analysis. However, even when

neglecting this system, significant differences in filtering efficiencies between both regions remain. FCO_2 from the North Sea estuaries (0.5 Tg C y^{-1}) is significantly lower than the 1.9 Tg C y^{-1} computed for the East coast of the US. The reason for the lower evasion rate in NW European estuaries is essentially twofold. First, the total cumulative surface area available for gas exchange is significantly lower along the North Sea, in spite of comparable flux densities calculated using the entire estuarine surface areas of both regions (14 mol C m^{-2} y^{-1} and 23 mol C m^{-2} y^{-1} for the East coast of the US and the North Sea, respectively). Second, although the overall riverine carbon loads are comparable in both regions (Fig. 11), the ratio of organic to inorganic matter input is much lower in the North Sea area because of the regional lithology is dominated by carbonate rocks and mixed sediments that contain carbonates (Dürr et al., 2005; Hartmann et al., 2012). As a consequence, TOC represents less than 20% of the riverine loads and only 10% of the carbon exported to the North Sea. In both regions, however, the increase of the inorganic to organic carbon ratio between input and output is sustained by a negative NEM (Fig. 11). Although the ratios themselves may significantly vary from a region of the world to the other as evidenced by these two studies, a NEM driven increase of the inorganic fraction within carbon load along the estuarine axis is consistent with the global estuarine carbon budget proposed by Bauer et al. (2013). In the East coast of the US, the respiration of riverine OC within the estuarine filter is partly compensated by OC inputs from marshes and mangroves in such a way that the input and export IC/OC ratios are closer than in the North Sea region.

3.4 Scope of applicability and model limitations

Complex multidimensional models are now increasingly applied to quantitatively explore carbon and nutrient dynamics along the land-ocean transition zone over seasonal and even annual timescales (Garnier et al., 2001; Arndt et al., 2007, 2009; Arndt and Regnier, 2007; Mateus et al., 2012). However, the application of such complex models remains limited to individual, well-constrained systems due their high data requirements and computational demand resulting from the need to resolve important physical, biogeochemical and geological processes on relevant temporal and

717 spatial scales. The one-dimensional, computationally efficient model C-GEM has been specifically
718 designed to reduce data requirements and computational demand and to enable regional/global
719 scale applications (Volta et al., 2014, 2016a). However, such a low data demand and computational
720 efficiency inevitably requires simplification. The following paragraphs critically discuss these
721 simplifications and their implications.

722 *Spatial resolution*

723 Here, C-GEM is used with a 0.5° spatial resolution. While this resolution captures the features of
724 large systems, it is still very coarse for relatively small watersheds, such as those of the St. Francis
725 River, Piscataqua River, May River or the Sapelo River. For instance, the 5 estuaries reported by Hunt
726 et al. (2010, 2011, see section 2.6) are all small systems covered by the same watershed at a 0.5°
727 resolution. Only watersheds whose area spans several grid cells can be properly identified and
728 represented (i.e. Merrimack or Penobscot with 6 and 9 cells, respectively).

729

730 *Hydrodynamic and Transport Model*

731 C-GEM is based on a theoretical framework that uses idealized geometries and significantly reduces
732 data requirements. These idealized geometries are fully described by three, easily obtainable
733 geometrical parameters (B, B0, H). The model thus approximates the variability of estuarine width
734 and cross-section along the longitudinal axis through a set of exponential functions. A
735 comprehensive sensitivity study (Volta et al., 2014) has shown that integrated process rates are
736 generally sensitive to changes in these geometrical parameters because of their control on estuarine
737 residence times. For instance, Volta et al. (2014) demonstrated that the NEM, is particularly sensitive
738 to the convergence length. Similarly, the use of constant depth profile may lead to variations of
739 about 10% in NEM (Volta et al., 2014). Nevertheless, geometrical parameters are generally easy to
740 constrain, especially well-monitored regions such as the US east coast. Here, all geometrical
741 parameters are constrained on the basis of observed estuarine surface areas and average water

depths. In addition, the model also accounts for the slope of the estuarine channel. This approach ensures that simulated estuarine surface areas, volumes and, thus, residence times are in good agreement with those of the real systems and minimizes uncertainties associated to the physical set-up.

In addition, the one-dimensional representation of the idealized estuarine systems does not resolve two- or three-dimensional circulation features induced by complex topography and density driven circulation. While C-GEM performs well in representing the dominant longitudional gradients, its applicability to branched systems or those with aspect ratios for which a dominant axis is difficult to identify (e.g. Blackwater estuary, UK; Pearl River estuary, China; Tagus estuary, Portugal; Bay of Brest, France) is limited.

Biogeochemical Model

Although the reaction network of C-GEM accounts for all processes that control estuarine FCO_2 (Borges and Abril, 2012; Cai, 2011), several, potentially important processes, such as benthic-pelagic exchange processes, phosphorous sorption/desorption and mineral precipitation, a more complex representation of the local phytoplankton community, grazing by higher trophic levels, or multiple reactive organic carbon pools are not included. Although these processes are difficult to constrain and their importance for FCO_2 is uncertain, the lack of their explicit representations induces uncertainties in Cfilt. In particular, the exclusion of benthic processes such as organic matter degradation and burial in estuarine sediments could result in an underestimation of Cfilt. However, because very little is known on the long term fate of organic carbon in estuarine sediments, setting up and calibrating a benthic module proves a difficult task. Furthermore, to a certain degree model parameters (such as organic matter degradation and denitrification rate constant) implicitly account for benthic dynamics. We nonetheless acknowledge that, by ignoring benthic processes and burial in particular, our estimates for the estuarine carbon filtering may be underestimated, particularly in the shallow systems of the SAR.

767 Biogeochemical model parameters for regional and global applications are notoriously difficult to
768 constrain (Volta et al., 2016b). Model parameters implicitly account for processes that are not
769 explicitly resolved and their transferability between systems is thus limited. In addition, published
770 parameter values are generally biased towards temperate regions in industrialized countries (Volta
771 et al., 2016b). A first order estimation of the parameter uncertainty associated to the estuarine
772 carbon removal efficiency (CFilt) can be extrapolated from the extensive parameter sensitivity
773 analyses carried out by Volta et al. (2014, 2016b). These comprehensive sensitivity studies on end-
774 member systems have shown that the relative variation in Cfilt when a number of key
775 biogeochemical parameters are varied by two orders of magnitude varies by ±15 % in prismatic
776 (short residence time on order of days) to ±25 % in funnel-shaped (long residence time) systems.
777 Thus, assuming that uncertainty increases linearly between those bounds as a function of residence
778 time, an uncertainty estimate can be obtained for each of our modelled estuary. With this simple
779 method, the simulated regional Cfilt of 1.9 Tg C yr-1 would be associated with an uncertainty range
780 comprised between 1.5 and 2.2 Tg C yr^{-1}. Our regional estuarine CO_2 evasion estimate is thus
781 reported with moderate confidence. Furthermore, in the future, this uncertainty range could be
782 further constrained using statistical methods such as Monte Carlo simulations (e.g. Lauerwald et al.,
783 2015).

784 *Boundary Conditions and Forcings*

785 In addition, simulations are only performed for climatological means over the period 1990-2010
786 without resolving interannual and secular variability. Boundary conditions and forcings are critical as
787 they place the modelled system in its environmental context and drive transient dynamics. However,
788 for regional applications, temporally resolved boundary conditions and forcings are difficult to
789 constrain. C-GEM places the lower boundary condition 20 km from the estuarine mouth into the
790 coastal ocean and the influence of this boundary condition on simulated biogeochemical dynamics is
791 thus limited. At the lower boundary condition, direct observations for nutrients and oxygen are

792 extracted from databases such as the World Ocean Atlas (Antonov et al., 2010). However, lower
793 boundary conditions for OC and pCO_2 (zero concentration for OC and assumption of pCO_2
794 equilibrium at the sea side) are simplified. This approach does not allow addressing the additional
795 complexity introduced by biogeochemical dynamics in the estuarine plume (see Arndt et al., 2011).
796 Yet, these dynamics only play a secondary role in the presented study that focuses on the role of the
797 estuarine transition zone in processing terrestrial-derived carbon.

798 Constraining upper boundary conditions and forcings is thus more critical. Here, C-GEM is forced by
799 seasonally-averaged conditions for Q, T, and radiation. To date, GlobalNEWS only provide yearly-
800 averaged conditions for a number of upper boundary conditions (Seitzinger et al., 2005; Mayorga et
801 al., 2010), representative of the year 2000. Simulations are thus only partly transient (induced by
802 seasonality in Q, T and radiation) and do not resolve short-lived events such as storms or extreme
803 drought conditions. In addition, direct observations of upper boundary conditions are rarely
804 available, in particular over seasonal or annual timescales. For the US East Coast estuaries, direct
805 observations are only available for O_2, Chlorophyll-a, DIC and Alk. For DIC and alkalinity boundary
806 conditions are constrained by calculating the average concentration over a period of about three
807 decades. In addition, observational data are extracted at the station closest to the model's upper
808 boundary, which might be still located several kilometres upstream or downstream of the model
809 boundary. Upper boundary conditions of POC, DOC, DIN, DIP, DSi are extracted from GlobalNews
810 and thus model-derived. As a consequence, our results are thus intimately dependent on the
811 robustness of the GlobalNEWS predictions. These values are usually only considered robust
812 estimates for watersheds larger than ~10 cells (Beusen et al., 2005), which only correspond to 13 of
813 the 42 estuaries modelled in this study.

814 *Model-data comparison*

815 The generic nature of the applied model approach renders a direct validation of model results on the
816 basis of local and instantaneous observational data (e.g. longitudinal profiles) difficult. In particular

817 the applications of seasonally/annually averaged or model-deduced boundary conditions, which are
818 likely not representative of these long-term average conditions, do not lend themselves well to
819 comparison with punctual measurements. Therefore, model performance is evaluated on the basis
820 of spatially aggregated estimates (e.g. regional FCO_2 estimates based on local measurements) rather
821 than system-to-system comparisons with longitudinal profile from specific days. However, note that
822 the performance of C-GEM has been intensively tested by specific model-data comparisons for a
823 number of different systems (e.g. Volta et al., 2014, 2016a) and we are thus confident of its
824 predictive capabilities.

825 Despite the numerous simplifying assumptions inevitably required for such a regional assessment of
826 carbon fluxes along the land-ocean continuum, the presented approach does nevertheless provide
827 an important step forward in evaluating the role of land-ocean transition systems in the global
828 carbon cycle. It provides a first robust estimate of carbon dynamics based on a theoretically well-
829 founded and carefully tested, spatially and temporally resolved model approach. This approach
830 provides novel insights that go beyond those gained through traditionally applied zero-salinity
831 method or box model approaches. In addition, it also highlights critical variables and data gaps and
832 thus helps guide efficient monitoring strategies.

833 **3.5 Towards predictors of the estuarine carbon processing**

834 The mutual dependence between geometry and transport in tidal estuaries and, ultimately, their
835 biogeochemical functioning (Savenije, 1992; Volta et al., 2014) allows relating easily extractable
836 parameters linked to their shape or their hydraulic properties to biogeochemical indicators. In this
837 section, we explore the relationships between such simple physical parameters and indicators of the
838 estuarine carbon processing $\overline{NEM}$, $\overline{FCO_2}$ and *CFilt*. In order to account for the effect of temperature
839 on C dynamics, -$\overline{NEM}$ and $\overline{FCO_2}$ are also normalized to the same temperature (arbitrarily chosen to
840 be 0 degree). These normalized values are obtained by dividing -$\overline{NEM}$ and $\overline{FCO_2}$ by a Q_{10} function
841 *f(T)* (see Volta et al., 2014). This procedure allows accounting for the exponential increase in the rate

of several temperature dependent processes contributing to the NEM (i.e. photosynthesis, organic carbon degradation…). Applying the same normalization to -$\overline{NEM}$ and $\overline{FCO_2}$ is a way of testing how intimately linked *NEM* and FCO_2 are in estuarine systems. Indeed linear relationships relating one to the other have been reported (Mayer and Eyre, 2012). The three indicators are then investigated as a function of the ratio between the estuarine surface *S* and the seasonal river discharge *Q*. The surface area is calculated from the estuarine width and length, as described by equation 2, in order to use a parameter which is potentially applicable to other regions for which direct estimates of the real estuarine surface area is not available. Since the fresh water residence time of a system is obtained by dividing volume by river discharge, the S/Q ratio is also intimately linked to residence time. Here, we choose to exclude the estuarine depth from the analysis because this variable cannot be easily quantified from maps or remote sensing images and would thus compromise the applicability of a predictive relationship on the global scale. However, from dimensional analysis, S/Q can be viewed as a water residence time normalized to meter depth of water. As shown by equation 3, *S* only requires constraining *B0* and width convergence length *b*, two parameters that can readily be extracted from the Google Earth engine. Global database of river discharges, as for instance RivDIS (Vörösmarty et al., 1996) are also available in such a way that the S/Q ratio can potentially be extracted for all estuaries around the globe.

Figure 12a reveals that small values of S/Q are associated with the most negative $\overline{NEM}$ / $f(T)$. The magnitude of the $\overline{NEM}$ then exponentially decreases with increasing values of S/Q. Estuaries characterized by small values of *S/Q* are mainly located in the NAR sub-region and correspond to small surface area, and thus short residence time systems. It is possible to quantitatively relate -$\overline{NEM}$ /$f(T)$ and S/Q through a power law function (y = 25.85 $x^{-0.64}$ with a r^2 = 0.82). The coefficient of determination remains the same when excluding estuaries from the NAR region and the equation itself is not significantly different, although those estuaries on their own do not display any statistically significant trend (Tab. 6). The decrease in the intensity of the net ecosystem metabolism

867 in larger estuaries (Fig 8), characterized by high S/Q ratios, can be related to the extensive
868 consumption of the organic matter pool during its transit through the estuarine filter. However,
869 when reported to the entire surface area of the estuary, larger systems (with high values of S/Q) still
870 reveal the most negative surface integrated *NEM* (Fig. 12b). It can also be noted that some estuaries
871 from the NAR region display very low values of *–NEM*. These data points correspond to fall and
872 winter simulations for which the temperature was relatively cold (<5 °C) and biogeochemical
873 processing was very low.

874 The overall response of $\overline{FCO_2}/f(T)$ to S/Q is comparable to that of -$\overline{NEM}/f(T)$ (Fig. 12c), with
875 lower values of $\overline{FCO_2}$ observed for high values of S/Q. However, for S/Q < 3 days m^{-1}, the $\overline{FCO_2}$
876 values are very heterogeneous and contain many, low $\overline{FCO_2}$ outliers from the NAR region. These
877 data points generally correspond to low water temperature conditions which keep pCO_2 low, even if
878 the system generates enough CO_2 internally via NEM. Thus, the well-documented correlation
879 between $\overline{NEM}$ and $\overline{FCO_2}$ (Maher and Eyre, 2012) does not seem to hold for systems with very short
880 residence times. For systems with S/Q > 3 days m^{-1}, we obtain a regression FCO_2 = -0.64 x *NEM* + 5.96
881 with a r^2 of 0.46, which compares well with the relation FCO_2 = -0.42 x *NEM* + 12 proposed by Maher
882 and Eyre (2012) who used 24 seasonal estimates from small Australian estuaries. However, our
883 results suggest that this relationship cannot be extrapolated to small systems such as those located
884 in the NAR. Figure 12d, which reports non-normalized FCO_2 reveals a monotonous increase of FCO_2
885 with S/Q. This suggests that, unlike the *NEM* for which the normalization by a temperature function
886 allowed explaining most of the variability; FCO_2 is mostly controlled by the water residence time
887 within the system. Discharge is the main FCO_2 driver in riverine dominated systems, while
888 interactions with marshes are driving the outgassing in marine dominated systems surrounded by
889 marshes. Net aquatic biological production (NEM being negative or near 0) in large estuaries (with
890 large S/Q) is another important reason for low FCO_2 in such systems. For example, despite the higher
891 CO_2 degassing flux in the upper estuary of the Delaware, strong biological CO_2 uptake in the mid-bay

892 and near zero NEM in the lower bay result in a much lower FCO_2 for the entire estuary (Joesoef et al.
893 2015). In systems with S/Q < 3 days m^{-1}, the short residence time prevents the excess CO_2 of
894 oversaturated water from being entirely exchanged with the atmosphere and simulations reveal that
895 the estuarine waters are still oversaturated in CO_2 at the estuarine mouth. Thus, the inorganic
896 carbon, produced by the decomposition of organic matter, is not outgassed within the estuary but
897 exported to the adjacent continental shelf waters. This result is consistent with the observation-
898 based hypothesis of Laruelle et al. (2015) for the NAR estuaries. As a consequence of the distinct
899 behavior of short residence time systems, the coefficient of determination of the best-fitted power
900 law function relating $\overline{FCO_2}$ and S/Q is only significant if NAR systems are excluded ($y = 31.64\ x^{-0.58}$
901 with a $r^2 = 0.70$). This thus suggests that such relationships (as well as that proposed by Maher and
902 Eyre, 2012) cannot be applied to any system but only those for which S/Q>3 day m^{-1}.

903 Finally, Fig. 12e reports the simulated mean seasonal carbon filtering capacities as a function of the
904 depth normalized residence time. Not surprisingly, and in overall agreement with previous studies
905 on nutrient dynamics in estuaries (Nixon et al., 1996), the carbon filtering capacity increases with
906 S/Q. The best statistical relation between *CFilt* and S/Q is obtained when including all 3 regions,
907 resulting in $r^2 = 0.70$ ($y = 40.64 \log_{10}(x) + 11.84$). Very little C removal occurs in systems with S/Q < 1
908 day m^{-1}. For systems characterized by longer depth-normalized residence times, *CFilt* increases
909 regularly, and reaches 100% for S/Q > 100 day m^{-1}. Such high values are only observed for very large
910 estuaries from the MAR region (Delaware and Chesapeake Bays); the majority of our systems had an
911 *S/Q* range between 1 and 100 day m^{-1}. The quantitative assessment of estuarine filtering capacities
912 is further complicated by the complex interplay of estuarine and coastal processes. Episodically,
913 marked spatial variability in concentration gradients near the estuarine mouth may lead to a reversal
914 of net material fluxes from coastal waters into the estuary (Regnier at al., 1998; Arndt et al. 2011).
915 Our results show that this feature is particularly significant for estuaries with a large width at the
916 mouth and short convergence length (funnel shaped or 'Bay type' systems). These coastal nutrient
917 and carbon inputs influence the internal estuarine C dynamics and lead to filtering capacities that

can exceed 100%. This feature is particularly significant in summer, when riverine inputs are low and the marine material is intensively processed inside the estuary.

Previous work investigated the relationship between fresh water residence time and nutrient retention (Nixon et al., 1996; Arndt et al., 2011; Laruelle, 2009). These studies, however, were constrained by the scarcity of data. For instance, the pioneering work of Nixon et al. (1996) only relied on a very limited number (<10) of quite heterogeneous coastal systems, all located along the North Atlantic. Here, our modeling approach allows us to generate 168 (42 x 4) data points, each representing a system-scale biogeochemical behavior. Together, this database spans the entire spectrum of estuarine settings and climatic conditions found along the East coast of the US. In addition, the ratio S/Q used as master variable for predicting temperature normalized -$\overline{NEM}$, $\overline{FCO_2}$ and *CFilt* only requires a few easily accessible geometric parameters (B0, b and L) and an estimate of the river discharge. While it is difficult to accurately predict $\overline{FCO_2}$ for small systems such as those located in the NAR region, the relationships found are quite robust for systems in which S/Q > 3 days m^{-1}. Most interestingly, *CFilt* values reveal a significant correlation with S/Q and could be used in combination with global riverine carbon delivery estimates such as GlobalNews 2 (Mayorga et al., 2010) to constrain the estuarine CO_2 evasion and the carbon export to the coastal ocean at the continental and global scales.

4. Conclusions

This study presents the first complete estuarine carbon budget for the East coast of the US using a modeling approach. The structure of the model C-GEM relies on a restricted number of readily available global datasets to constrain boundary conditions and limits the number of geometrical and physical parameters to be constrained. Our simulations predict a total CO_2 outgassing of 1.9 Tg C y^{-1} for all tidal estuaries of the East coast of the US. This quantification accounts for the seasonality in estuarine carbon processing as well as for distinct individual behaviors among estuarine types (marine or river dominated). The total carbon output to the coastal ocean is estimated at 2.7 TgC y^{-1},

943 and the carbon filtering capacity with respect to riverine, marshes and mangrove inputs is thus on
944 the order of 40%. This value is significantly higher than the recently estimated C filtering capacity for
945 estuaries surrounding the North Sea using a similar approach (Volta et al., 2016a), mainly because
946 the surface area available for gas exchange and the draining lithology limits the CO_2 evasion in the
947 NW European systems. At the regional scale of the US East coast estuaries, net heterotrophy is the
948 main driver (50%) of the CO_2 outgassing, followed by the ventilation of riverine supersaturated
949 waters entering the estuarine systems (32%) and nitrification (18%). The dominant mechanisms for
950 the gas exchange and the resulting carbon filtering capacities nevertheless reveal a clear latitudinal
951 pattern, which reflects the shapes of estuarine systems, climatic conditions and dominant land-use
952 characteristics.

953 Our model results are used to derive predictive relationships relating the intensity of the area-based
954 Net Ecosystem Metabolism ($\overline{NEM}$), air-water CO_2 exchange ($\overline{FCO_2}$) and the carbon filtering capacity
955 (*CFilt*) to the depth normalized residence time, expressed as the ratio of the estuarine surface area
956 to the river discharge. In the future, such simple relationships relying on readily available geometric
957 and hydraulic parameters could be used to quantify carbon processing in areas of the world devoid
958 of direct measurements. However, it is important to note that such simple relationships are only
959 valid over the range of boundary conditions and forcings explored and may not be applicable to
960 conditions that fall outside of this range. In regions with better data coverage, such as the one
961 investigated here, our study highlights that the regional-scale quantification, attribution, and
962 projection of estuarine biogeochemical cycling are now at reach.

963 **5. Acknowledgements**

964 G. G. Laruelle is Chargé de recherches du F.R.S.-FNRS at the Université Libre de Bruxelles. The
965 research leading to these results has received funding from the European Union's Horizon 2020
966 research and innovation programme under the Marie Sklodowska-Curie grant agreement No 643052

967 (C-CASCADES project). The authors thank V. L. Mulder for her thorough reading of the manuscript
968 upon submission.

969

970 **References:**

971 Abril, G., Nogueira, M., Etcheber, H., Cabeçadas, G., Lemaire, E., and Brogueira, M.J.: Behaviour of
972 organic carbon in nine contrasting European estuaries. Estuar. Coast. Shelf Sci., 54, 241-262,
973 2002.
974 Antonov, J.I., Seidov, D., Boyer, T.P., Locarnini, R.A., Mishonov, A.V., Garcia, H.E., Baranova, O.K.,
975 Zweng, M.M., and Johnson, D.R.: World Ocean Atlas 2009, Volume 2: Salinity. S., 2010.
976 Arndt, S., Vanderborght, J.P., and Regnier, P.: Diatom growth response to physical forcing in a
977 macrotidal estuary: Coupling hydrodynamics, sediment transport, and biogeochemistry.
978 Journal of Geophysical Research C: Oceans, 112(5), 2007.
979 Arndt, S. and Regnier, P.: A model for the benthic-pelagic coupling of silica in estuarine ecosystems:
980 sensitivity analysis and system scale simulation, Biogeosciences, 4, 331–352, doi:10.5194/bg-
981 4-331-2007, 2007.
982 Arndt, S., Regnier, P., and Vanderborght, J.P.: Seasonally-resolved nutrient export fluxes and filtering
983 capacities in a macrotidal estuary. Journal of Marine Systems, 78(1), 42-58, 2009.
984 Arndt, S., Lacroix, G., Gypens, N., Regnier, P., and Lancelot, C.: Nutrient dynamics and phytoplankton
985 development along an estuary-coastal zone continuum: A model study. Journal of Marine
986 Systems, 84(3-4), 49-66, 2011.
987 Atlas, R., Hoffman, R.N., Ardizzone, J., Leidner, S.M., Jusem, J.C., Smith, D.K. and Gombos, D.: A
988 cross-calibrated, multiplatform ocean surface wind velocity product for meteorological and
989 oceanographic applications. Bulletin of the American Meteorological Society, 92(2), 157-174,
990 2011.
991 Baklouti, M., Chevalier, C., Bouvy, M., Corbin, D., Pagano, M., Troussellier, M., and Arfi, R.: A study of
992 plankton dynamics under osmotic stress in the Senegal River Estuary, West Africa, using a 3D
993 mechanistic model, Ecol. Model., 222, 2704–2721, 2011.
994 Bauer, J.E., Cai, W.J., Raymond, P.A., Bianchi, T.S., Hopkinson, C.S., and Regnier, P.A.G.: The changing
995 carbon cycle of the coastal ocean. Nature, 504(7478), 61-70, 2013.
996 Beusen, A. H.W., Dekkers, A. L. M., Bouwman, A. F., Ludwig,W., and Harrison, J.: Estimation of global
997 river transport of sediments and associated particulate C, N, and P, Global Biogeochem. Cy.,
998 19, GB4S05, doi:10.1029/2005GB002453, 2005.
999 Beusen, A.H.W., Bouwman, A.F., Dürr, H.H., Dekkers, A.L.M., and Hartmann, J.: Global patterns of
1000 dissolved silica export to the coastal zone: Results from a spatially explicit global model.
1001 Global Biogeochemical Cycles, 23, GB0A02, doi:10.1029/2008GB003281, 2009.
1002 Borges, A.V., Delille, B., and Frankignoulle, M.: Budgeting sinks and sources of CO_2 in the coastal
1003 ocean: Diversity of ecosystems counts. Geophys. Res. Lett., 32(14), L14601, 2005.
1004 Borges, A.V., and Abril, G.: Carbon Dioxide and Methane Dynamics in Estuaries. In: E. Wolanski and
1005 D.S. McLusky (Editors), Treatise on Estuarine and Coastal Science. Academic Press, Waltham,
1006 pp. 119–161, 2012.
1007 Bricker, S., Longstaff, B., Dennison, W., Jones, A., Boicourt, K., Wicks, C., and Woerner, J.: Effects of
1008 Nutrient Enrichment In the Nation's Estuaries: A Decade of Change, NOAA, MD, 2007.
1009 Brock, T.D.: Calculating solar radiation for ecological studies. Ecological Modelling, 14(1-2), 1-19,
1010 1981.
1011 Caffrey, J.: Factors controlling net ecosystem metabolism in U.S. estuaries. Estuaries, 27(1), 90-101,
1012 2004.
1013 Cai, W.J., and Wang, Y.: The chemistry, fluxes, and sources of carbon dioxide in the estuarine waters
1014 of the Satilla and Altamaha Rivers, Georgia. Limnology and Oceanography, 43(4), 657-668,
1015 1998.
1016 Cai, W.J., Wang, Y., and Hodson, R. E.: Acid-base properties of dissolved organic matter in the
1017 estuarine waters of Georgia, USA. Geochimica et Cosmochimica Acta, 62(3), 473-483, 1998.
1018 Cai, W.J., Pomeroy, L.R., Moran, M.A., and Wang, Y.: Oxygen and carbon dioxide mass balance for
1019 the estuarine-intertidal marsh complex of five rivers in the southeastern U.S. Limnology and
1020 Oceanography, 44, 639-649, 1999.

Cai, W.J.: Estuarine and coastal ocean carbon paradox: CO_2 sinks or sites of terrestrial carbon incineration? Ann. Rev. Mar. Sci., 3, 123-145, 2011.

Cerco, C., Kim, S.-C., and Noel, M.: The 2010 Chesapeake Bay eutrophication model. US Environmental Protection Agency Chesapeake Bay Program, Annapolis, MD, 2010.

Chen, C.-T.A., Huang, T.-H., Fu, Y.-H., Bai, Y., and He, X.: Strong sources of CO2 in upper estuaries become sinks of CO2 in large river plumes. Current Opinion in Environmental Sustainability, 4(2), 179-185, 2012.

Chen, C.-T. A., Huang, T.-H., Chen, Y.-C., Bai, Y., He, X., and Kang, Y.: Air-sea exchanges of CO2 in the world's coastal seas, Biogeosciences, 10, 6509–6544, doi:10.5194/bg-10-6509-2013, 2013.

Dai, T., and Wiegert, R.G.: Estimation of the primary productivity of Spartina alterniflora using a canopy model. Ecography, 19(4), 410-423, 1996.

Dürr, H.H., Meybeck, M., and Dürr, S.H.: Lithological composition of the Earth's continental surfaces derived from a new digital map emphasizing riverine material transfer. Glob. Biogeochem. Cycles 19 (4), GB4S10, 2005.

Dürr, H.H., Laruelle, G.G., van Kempen, C.M., Slomp, C.P., Meybeck, M., and Middelkoop, H.: Worldwide Typology of Nearshore Coastal Systems: Defining the Estuarine Filter of River Inputs to the Oceans. Estuaries and Coasts, 34(3), 441-458, 2011.

EPA (2009). "1970 - 2008 Average annual emissions, all criteria pollutants in MS Excel." National Emissions Inventory (NEI) Air Pollutant Emissions Trends Data. Office of Air Quality Planning and Standards. Available online at <http://www.epa.gov/ttn/chief/trends/index.html>

Fekete, B.M., Vörösmarty, C.J., and Grabs, W.: High-resolution fields of global runoff combining observed river discharge and simulated water balances. Global Biogeochemical Cycles, 16(3), 15-1, 2002.

Fischer, H. B.: Mixing and Dispersion in Estuaries, Annu. Rev. Fluid Mech., 8, 107–133, 1976.

Friedrichs, M.A.M., and Hofmann, E.E.: Physical control of biological processes in the central equatorial Pacific Ocean. Deep-Sea Research Part I: Oceanographic Research Papers, 48(4), 1023-1069, 2001.

Garcia, H.E., Locarnini, R.A., Boyer, E.W., Antonov, A., Baranova, O.K., Zweng, M.M., and Johnson, D.R.: World Ocean Atlas 2009, Volume 3: Dissolved Oxygen, Apparent Oxygen Utilization, and Oxygen Saturation, 2010a.

Garcia, H.E., Locarnini, R.A., Boyer, E.W., Antonov, J.I., Baranova, O.K., Zweng, M.M., and Johnson, D.R.: World Ocean Atlas 2009, Volume 4: Nutrients (phosphate, nitrate, silicate), 2010b.

Garnier, J., Servais, P., Billen, G., Akopian, M., and Brion, N.: Lower Seine River and Estuary (France) Carbon and Oxygen Budgets During Low Flow, Estuaries, 24, 964–976, 2001.

GRDC: Global Freshwater Fluxes into the World Oceans / Online provided by Global Runoff Data Centre. 2014 ed. Koblenz: Federal Institute of Hydrology (BfG), 2014.

Harrison, J.A., Caraco, N., and Seitzinger, S.P.: Global patterns and sources of dissolved organic matter export to the coastal zone: Results from a spatially explicit, global model. Global Biogeochemical Cycles, 19(4), GB4S03, doi:10.1029/2004GB002357, 2005.

Hartmann, J., Jansen, N., Dürr, H.H., Kempe, S., and Köhler, P.: Global CO_2 consumption by chemical weathering: What is the contribution of highly active weathering regions? Global Planet. Change, 69(4), 185-194, 2009.

Hartmann, J., Dürr, H.H., Moosdorf, N., Meybeck, M., and Kempe, S.: The geochemical composition of the terrestrial surface (without soils) and comparison with the upper continental crust. Int. J. Earth Sci. 101, 365-376, 2012.

Herrmann, M., Najjar, R.G., Kemp, W.M., Alexander, R.B., Boyer, E.W., Cai, W.-J., Griffith, P.C., Kroeger, K.D., McCallister, S.L., and Smith, R.A.: Net ecosystem production and organic carbon balance of U.S. East Coast estuaries: A synthesis approach, Global Biogeochem. Cycles, 29, doi:10.1002/2013GB004736, 2015.

Hofmann, A.F., Soetaert, K., and Middelburg, J.J.: Present nitrogen and carbon dynamics in the Scheldt estuary using a novel 1-D model. Biogeosciences, 5(4), 981-1006, 2008.

Hofmann, E.E., Cahill, B., Fennel, K., Friedrichs, M.A.M., Hyde, K., Lee, C., Mannino, A., Najjar, R.G., O'Reilly, J.E., Wilkin, J., and Xue, J.: Modeling the dynamics of continental shelf carbon. Ann Rev Mar Sci. 3, 93-122, 2011.

Hunt, C. W., Salisbury, J. E., Vandemark, D., and McGillis, W.: Contrasting Carbon Dioxide Inputs and Exchange in Three Adjacent New England Estuaries. Estuar. Coast., 34, 68–77, doi:10.1007/s12237-010-9299-9, 2010.

Hunt, C.W., Salisbury, J.E., Vandemark, D., and McGillis, W.: Contrasting Carbon Dioxide Inputs and Exchange in Three Adjacent New England Estuaries. Estuaries and Coasts, 34(1), 68-77, 2011.

Ippen, A.T., and Harleman, D.R.F.: One-dimensional Analysis of Salinity Intrusion in Estuaries, Technical Bulletin No. 5, Committee on Tidal Hydraulics, Corps of Engineers, US Army, Vicksburg, 1961.

Jiang, L.Q., Cai, W.J., and Wang, Y.: A comparative study of carbon dioxide degassing in river- and marine-dominated estuaries. Limnology and Oceanography, 53(6), 2603-2615, 2008.

Jiang, L.-Q., Cai, W.-J., Wang, Y., and Bauer, J. E.: Influence of terrestrial inputs on continental shelf carbon dioxide, Biogeosciences, 10, 839–849, doi:10.5194/bg-10-839-2013, 2013.

Joesoef, A., Huang, W.-J., Gao, Y., and Cai, W.-J.: Air–water fluxes and sources of carbon dioxide in the Delaware Estuary: spatial and seasonal variability, Biogeosciences, 12, 6085-6101, doi:10.5194/bg-12-6085-2015, 2015.

Kent, B.H.: Turbulent diffusion in a Sectionally Homogeneous Estuary, Technical Report 16, Chesapeake Bay Institute, John Hopkins, University, Baltimore, 1958.

Key, R.M., Kozyr, A., Sabine, C.L., Lee, K., Wanninkhof, R., Bullister, J.L., Feely, R.A., Millero, F.J., Mordy, C., and Peng, T.H.: A global ocean carbon climatology: Results from Global Data Analysis Project (GLODAP). Global Biogeochemical Cycles, 18(4), 1-23, 2004.

Laruelle, G.G.: Quantifying nutrient cycling and retention in coastal waters at the global scale, Ph D dissertation, Utrecht University, 2009.

Laruelle, G. G., Regnier, P., Ragueneau, O., Kempa, M., Moriceau, B., Ni Longphuirt, S., Leynaert, A., Thouzeau, G., and Chauvaud, L.: Benthic-pelagic coupling and the seasonal silica cycle in the Bay of Brest (France): new insights from a coupled physical-biological model, Mar. Ecol.-Prog. Ser., 385, 15–32, 2009.

Laruelle, G.G., Dürr, H.H., Slomp, C.P., and Borges, A.V.: Evaluation of sinks and sources of CO_2 in the global coastal ocean using a spatially-explicit typology of estuaries and continental shelves. Geophys. Res. Lett., 37(15), L15607, doi:10.1029/2010GL043691, 2010.

Laruelle, G.G., Dürr, H.H., Lauerwald, R., Hartmann, J., Slomp, C.P., Goossens, N., and Regnier, P.A.G.: Global multi-scale segmentation of continental and coastal waters from the watersheds to the continental margins. Hydrol. Earth Syst. Sci., 17(5), 2029-2051, 2013.

Laruelle, G.G., Lauerwald, R., Rotschi, J. Raymond, P.A., and Regnier, P.: Seasonal response of air-water CO2 exchange along the land-ocean aquatic continuum of the northeast North American coast. Biogeosci. 12, 1447-1458, 2015.

Lauerwald, R., Hartmann, J., Moosdorf, N., Kempe, S., and Raymond, P.A.: What controls the spatial patterns of the riverine carbonate system? — A case study for North America. Chemical Geology, 337–338, 114-127, 2013.

Lauerwald, R., Laruelle, G. G., Hartmann, J., Ciais, P., and Regnier, P. A. G.: Spatial patterns in CO2 evasion from the global river network, Global Biogeochem. Cy., 29, 534–554, doi:10.1002/2014GB004941, 2015.

Leonard, B.: Third-Order Upwinding as a Rational Basis for Computational Fluid Dynamics, in: Computational Techniques and Applications: CTAC-83, edited by: Noye J. and Fletcher C. A. J., Elsevier, North-Holland, 1984.

Le Quéré, C., Peters, G. P., Andres, R. J., Andrew, R. M., Boden, T. A., Ciais, P., Friedlingstein, P., Houghton, R. A., Marland, G., Moriarty, R., Sitch, S., Tans, P., Arneth, A., Arvanitis, A., Bakker, D. C. E., Bopp, L., Canadell, J. G., Chini, L. P., Doney, S. C., Harper, A., Harris, I., House, J. I., Jain, A. K., Jones, S. D., Kato, E., Keeling, R. F., Klein Goldewijk, K., Körtzinger, A., Koven, C.,

Lefèvre, N., Maignan, F., Omar, A., Ono, T., Park, G.-H., Pfeil, B., Poulter, B., Raupach, M. R., Regnier, P., Rödenbeck, C., Saito, S., Schwinger, J., Segschneider, J., Stocker, B. D., Takahashi, T., Tilbrook, B., van Heuven, S., Viovy, N., Wanninkhof, R., Wiltshire, A., and Zaehle, S.: Global carbon budget 2013, Earth Syst. Sci. Data, 6, 235-263, doi:10.5194/essd-6-235-2014, 2014.

Le Quéré, C., Moriarty, R., Andrew, R. M., Canadell, J. G., Sitch, S., Korsbakken, J. I., Friedlingstein, P., Peters, G. P., Andres, R. J., Boden, T. A., Houghton, R. A., House, J. I., Keeling, R. F., Tans, P., Arneth, A., Bakker, D. C. E., Barbero, L., Bopp, L., Chang, J., Chevallier, F., Chini, L. P., Ciais, P., Fader, M., Feely, R. A., Gkritzalis, T., Harris, I., Hauck, J., Ilyina, T., Jain, A. K., Kato, E., Kitidis, V., Klein Goldewijk, K., Koven, C., Landschützer, P., Lauvset, S. K., Lefèvre, N., Lenton, A., Lima, I. D., Metzl, N., Millero, F., Munro, D. R., Murata, A., Nabel, J. E. M. S., Nakaoka, S., Nojiri, Y., O'Brien, K., Olsen, A., Ono, T., Pérez, F. F., Pfeil, B., Pierrot, D., Poulter, B., Rehder, G., Rödenbeck, C., Saito, S., Schuster, U., Schwinger, J., Séférian, R., Steinhoff, T., Stocker, B. D., Sutton, A. J., Takahashi, T., Tilbrook, B., van der Laan-Luijkx, I. T., van der Werf, G. R., van Heuven, S., Vandemark, D., Viovy, N., Wiltshire, A., Zaehle, S., and Zeng, N.: Global Carbon Budget 2015, Earth Syst. Sci. Data, 7, 349-396, doi:10.5194/essd-7-349-2015, 2015.

Lin, J., Xie, L., Pietrafesa, L. J., Ramus, J. S., and Paerl, H.W.: Water Quality Gradients across Albemarle-Pamlico Estuarine System: Seasonal Variations and Model Applications, J. Coast. Res., 23, 213–229, 2007.

Locarnini, R.A., Mishonov, A.V., Antonov, J.I., Boyer, T.P., Garcia, H.E., Baranova, O.K., Zweng, M.M., and Johnson, D.R.: World Ocean Atlas 2009, Volume 1: Temperature, 2010.

Ludwig, W., Probst, J. L., and Kempe, S.: predicting the oceanic input of organic carbon by continental erosion, Global Bio geochem. Cy., 10, 23–41, 1996.

Maher, D.T., and Eyre, B.D.: Carbon budgets for three autotrophic Australian estuaries: Implications for global estimates of the coastal air-water CO2 flux. Global Biogeochem. Cycles, 26(1), GB1032, 2012.

Mateus, M., Vaz, N., and Neves, R.: A process-oriented model of pelagic biogeochemistry for marine systems. Part II: Application to a mesotidal estuary, J. Mar. Syst., 94, 90–101, 2012.

Mayorga, E., Seitzinger, S.P., Harrison, J.A., Dumont, E., Beusen, A.H.W., Bouwman, A.F., Fekete, B.M., Kroeze, C., and Van Drecht, G.: Global Nutrient Export from WaterSheds 2 (NEWS 2): Model development and implementation. Environmental Modelling and Software, 25(7), 837-853, 2010.

Meybeck, M.: Carbon, nitrogen, and phosphorus transport by world rivers. Am. J. Sci., 282(4), 401-450, 1982.

Meybeck, M., Dürr, H. H., and Vörosmarty, C. J.: Global coastal segmentation and its river catchment contributors: A new look at land-ocean linkage, Global Biogeochem. Cy., 20, GB1S90, doi:10.1029/2005GB002540, 2006.

Middelburg, J.J., Klaver, G., Nieuwenhuize, J., Wielemaker, A., De Haas, W., Vlug, T., and Van Der Nat, J.F.W.A.: Organic matter mineralization in intertidal sediments along an estuarine gradient. Marine Ecology Progress Series, 132(1-3), 157-168, 1996.

NASA/NGA: SRTM Water Body Data Product Specific Guidance, Version 2.0, 2003.

Najjar, R.G., Friedrichs, M., and Cai, W.-J. (Editors): Report of The U.S. East Coast Carbon Cycle Synthesis Workshop, January 19-20, 2012. Ocean Carbon and Biogeochemistry Program and North American Carbon Program, 34 pp, 2012.

Nihoul, J. C. J., and Ronday, F.: Modèles d'estuaires partiellement stratifiés, Projet Mer, Vol. 10, Service de la Programmation Scientifique, Bruxelles, Belgium, 71–98, 1976.

Nixon, S.W., J.W. Ammerman, L.P. Atkinson, V.M. Berounsky, G. Billen, W.C. Boicourt, W.R. Boynton, T.M. Church, D.M. Ditoro, R. Elmgren, J.H. Garber, A.E. Giblin, R.A. Jahnke, N.J. P. Owens, M.E.Q. Pilson, and Seitzinger, S.P.: The fate of nitrogen and phosphorus at the land–sea margin of the North Atlantic Ocean. Biogeochemistry 3, 141–180, 1996.

NOAA: National Estuarine Inventory Data Atlas, Volume 1: Physical and Hydrologic Characteristics, National Oceanic and Atmospheric Administration, MD, 1985.
Odum, H.T.: Primary Production in Flowing Waters. Limnol. Oceanogr., 1, 102-117, 1956.
O'Kane, J. P.: Estuarine Water Quality Management. Pitman, London, U.K, 1980.
Platt, T., Gallegos, C. L., and Harrison, W. G.: Photoinhibition of photosynthesis in natural assemblages of marine phytoplankton. J. Mar. Res., 38, 687-701, 1980.
Preddy, W. S.: The mixing and movement of water in the estuary of the Thames, J. Mar. biol. Ass. UK, 33, 645–662, 1954.
Press, W. H., Teukolosky, S. A., Vetterling, W. T., and Flannery, B.P.: Numerical Recipes in C: The Art of Scientific Programming, 2nd Edn., Cambridge University Press, USA, 1992.
Pritchard, D. W.: The Equations of Mass Continuity and Salt Continuity in Estuaries, J. Marine Res., 15, 33–42, 1958.
Raymond, P.A., Caraco, N.F., and Cole, J.J.: Carbon dioxide concentration and atmospheric flux in the Hudson River. Estuaries, 20(2), 381-390, 1997.
Raymond, P.A., Bauer, J.E., and Cole, J.J.: Atmospheric CO2 evasion, dissolved inorganic carbon production, and net heterotrophy in the York River estuary. Limnology and Oceanography, 45(8), 1707-1717, 2000.
Raymond, P.A., and Hopkinson, C.S.: Ecosystem Modulation of Dissolved Carbon Age in a Temperate Marsh-Dominated Estuary. Ecosystems, 6(7), 694-705, 2003.
Raymond, P.A., Hartmann, J., Lauerwald, R., Sobek, S., McDonald, C., Hoover, M., Butman, D., Striegl, R., Mayorga, E., Humborg, C., Kortelainen, P., Dürr, H., Meybeck, M., Ciais, P., and Guth, P.: Global carbon dioxide emissions from inland waters. Nature, 503(7476), 355-359, 2013.
Regnier, P., Wollast, R., and Steefel, C.I.: Long-term fluxes of reactive species in macrotidal estuaries: Estimates from a fully transient, multicomponent reaction-transport model. Marine Chemistry, 58(1-2), 127-145, 1997.
Regnier, P., Mouchet, A., Wollast, R., and Ronday, F.: A discussion of methods for estimating residual fluxes in strong tidal estuaries, Cont. Shelf Res., 18, 1543–1571, 1998.
Regnier, P., and Steefel, C.I.: A high resolution estimate of the inorganic nitrogen flux from the Scheldt estuary to the coastal North Sea during a nitrogen-limited algal bloom, spring 1995. Geochimica et Cosmochimica Acta, 63(9), 1359-1374, 1999.
Regnier, P., Vanderborght, J. P., Steefel, C. I., and O'Kane, J. P.: Modeling complex multi-component reactive-transport systems: Towards a simulation environment based on the concept of a Knowledge Base, Appl. Math. Model., 26, 913–927, 2002.
Regnier, P., Friedlingstein, P., Ciais, P., Mackenzie, F.T., Gruber, N., Janssens, I.A., Laruelle, G.G., Lauerwald, R., Luyssaert, S., Andersson, A.J., Arndt, S., Arnosti, C., Borges, A.V., Dale, A.W., Gallego-Sala, A., Godderis, Y., Goossens, N., Hartmann, J., Heinze, C., Ilyina, T., Joos, F., LaRowe, D.E., Leifeld, J., Meysman, F.J.R., Munhoven, G., Raymond, P.A., Spahni, R., Suntharalingam, P., and Thullner, M.: Anthropogenic perturbation of the carbon fluxes from land to ocean. Nature Geosci, 6(8), 597-607, 2013a.
Regnier, P., Arndt, S., Goossens, N., Volta, C., Laruelle, G.G., Lauerwald, R., and Hartmann, J.: Modelling Estuarine Biogeochemical Dynamics: From the Local to the Global Scale. Aquatic Geochemistry, 19(5-6), 591-626, 2013b.
Riemann, B., Simonsen, P., and Stensgaard, L.: The carbon and chlorophyll content of phytoplankton from various nutrient regimes. Journal of Plankton Research, 11 (5), 1037-1045, 1989.
Rossow, W.B., and Schiffer, R.A.: Advances in understanding clouds from ISCCP. Bull. Amer. Meteorol. Soc., 80, 2261-2288, doi:10.1175/1520-0477(1999)080<2261:AIUCFI>2.0.CO;2, 1999.
Sarma, V.V.S.S., Viswanadham, R., Rao, G.D., Prasad, V.R., Kumar, B.S.K., Naidu, S.A., Kumar, N.A., Rao, D.B., Sridevi, T., Krishna, M.S., Reddy, N.P.C., Sadhuram, Y., and Murty, T.V.R.: Carbon dioxide emissions from Indian monsoonal estuaries. Geophysical Research Letters, 39(3), L03602, 2012.

Savenije, H.H.G.: A one-dimensional model for salinity intrusion in alluvial estuaries. Journal of Hydrology, 85(1-2), 87-109, 1986.
Savenije, H.H.G.: Lagrangian solution of St. Venant's equations for alluvial estuary. Journal of Hydraulic Engineering, 118(8), 1153-1163, 1992.
Savenije, H. H. G. (Ed.): Salinity and Tides in Alluvial Estuaries, 1st Edn., Elsevier, Amsterdam, 2005.
Savenije, H. H. G. (Ed.): Salinity and Tides in Alluvial Estuaries, 2nd Edn., available at: http://salinityandtides.com (last access: 8 March 2015), 2012.
Seitzinger, S. P., Harrison, J. A., Dumont, E., Beusen, A. H. W., and Bouwman, A. F.: Sources and delivery of carbon, nitrogen, and phosphorus to the coastal zone: An overview of Global Nutrient Export from Watersheds (NEWS) models and their application, *Global Biogeochem. Cycles*, 19, GB4S01, doi:10.1029/2005GB002606, 2005.
Schwarz, G.E., Hoos, A.B., Alexander, R.B., and Smith, R.A.: The SPARROW Surface Water-Quality Model: Theory, Application and User Documentation. U.S. Geological Survey, Techniques and Methods Report, Book 6, Chapter B3, Reston, Virginia, 2006
Sharp, J. H., Yoshiyama, K., Parker, Schwartz, M. C., Curless, S. E., Beauregard, A. Y., Ossolinski, J. E., and Davis, A. R.: A Biogeochemical View of Estuarine Eutrophication: Seasonal and Spatial Trends and Correlations in the Delaware Estuary. Estuaries and Coasts, 32, 1023-1043,. doi:10.1007/s12237-009-9210-8, 2009.
Sharp, J. H.: Estuarine oxygen dynamics: What can we learn about hypoxia from long-time records in the Delaware Estuary? Limnol. Oceanogr., 55(2), 2010, 535–548, 2010.
Shih, J.-S., Alexander, R.B., Smith, R.A., Boyer, E.W., Schwarz, G.E., and Chung, S.: An initial SPARROW model of land use and in-stream controls on total organic carbon in streams of the conterminous United States, U. S. Geological Survey, Reston, Virginia, 2010.
Signorini, S.R., Mannino, A., Najjar Jr, R.G., Friedrichs, M.A.M., Cai, W.J., Salisbury, J., Wang, Z.A., Thomas, H., and Shadwick, E.: Surface ocean pCO2 seasonality and sea-air CO2 flux estimates for the North American east coast. Journal of Geophysical Research C: Oceans, 118(10), 5439-5460, 2013.
Simmons, H. B.: Some effects of inland discharge on estuarine hydraulics, Proc. Am. Soc. Civ. Eng.-ASCE, 81, 792, 1955.
Soetaert, K., and Herman, P.M.J.: Nitrogen dynamics in the Westerschelde estuary (SW Netherlands) estimated by means of the ecosystem model MOSES. Hydrobiologia, 311(1-3), 225-246, 1995.
Stets, E.G., and Strieg, R.G.: Carbon export by rivers draining the conterminous united states. Inland Waters, 2(4), 177-184, 2012.
Stigter, C., and Siemons, J.: Calculation of longitudinal salt distribution in estuaries as function of time, Publication Delft Hydraulics Laboratory, 52, The Netherlands, 1967.
Tian, H., Chen, G., Liu, M., Zhang, C., Sun, G., Lu, C., Xu, X., Ren, W., Pan, S., and Chappelka, A.: Model estimates of net primary productivity, evapotranspiration, and water use efficiency in the terrestrial ecosystems of the southern United States during 1895-2007. Forest Ecology and Management, 259(7), 1311-1327, 2010.
Tian, H., Chen, G., Zhang, C., Liu, M., Sun, G., Chappelka, A., Ren, W., Xu, X., Lu, C., Pan, S., Chen, H., Hui, D., McNulty, S., Lockaby, G., and Vance, E.: Century-Scale Responses of Ecosystem Carbon Storage and Flux to Multiple Environmental Changes in the Southern United States. Ecosystems, 15(4), 674-694, 2012.
U. S. Fish and Wildlife Service. 2014. National Wetlands Inventory website. U.S. Department of the Interior, Fish and Wildlife Service, Washington, D.C. http://www.fws.gov/wetlands/, last accessed: February 2015.
Vanderborght, J.P., Wollast, R., Loijens, M., and Regnier, P.: Application of a transport-reaction model to the estimation of biogas fluxes in the Scheldt Estuary. Biogeochemistry, 59(1-2), 207-237, 2002.

1274 Vanderborght, J.P., Folmer, I., Aguilera, D.R., Uhrenholdt, T., and Regnier, P.: Reactive-transport
1275 modelling of a river-estuarine-coastal zone system: application to the Scheldt estuary. Mar.
1276 Chem. 106, 92-110, 2007.
1277 Volta, C., Arndt, S., Savenije, H.H.G., Laruelle, G.G., and Regnier, P.: C-GEM (v 1.0): a new, cost-
1278 efficient biogeochemical model for estuaries and its application to a funnel-shaped system.
1279 Geosci. Model Dev., 7, 1271-1295, doi:10.5194/gmd-7-1271-2014, 2014.
1280 Volta, C., Laruelle, G. G., and Regnier, P.: Regional carbon and CO_2 budgets of North Sea tidal
1281 estuaries, Estuarine, Coastal and Shelf Science, 176, 76-90, 2016a.
1282 Volta, C., Laruelle, G. G., Arndt, S., and Regnier, P.: Linking biogeochemistry to hydro-geometrical
1283 variability in tidal estuaries: a generic modeling approach, Hydrol. Earth Syst. Sci., 20, 991-
1284 1030, doi:10.5194/hess-20-991-2016, 2016b.
1285 Vörösmarty, C.J., Fekete, B., and Tucker, B.A.: River Discharge Database, Version 1.0 (RivDIS v1.0),
1286 Volumes 0 through 6. A contribution to IHP-V Theme 1. Technical Documents in Hydrology
1287 Series. UNESCO, Paris, 1996.
1288 Wang, Z.A., and Cai, W.J.: Carbon dioxide degassing and inorganic carbon export from a marsh-
1289 dominated estuary (the Duplin River): A marsh CO2 pump. Limnology and Oceanography,
1290 49(2), 341-354, 2004.
1291 Zeebe, R. E. and Wolf-Gladrow, D. (Eds.): CO2 in seawater: equilibrium, kinetics, isotopes, Elsevier,
1292 Amsterdam, 2001.

1293

Table 1: Estimates of total annual riverine input from watersheds to estuaries (Tg C yr^{-1}). The ranges are based on Stets and Striegl (2012), Global NEWS (Mayorga et al. 2010), Hartmann et al. (2009), SPARROW (Shih et al. 2010) and DLEM (Tian et al. 2010, 2012). Modified from Najjar et al. 2012.

	DIC	**DOC**	**POC**	**TOTAL**
NAR	0.2-0.8	0.3-2.1	0.1-0.2	0.6-3.1
MAR	1.4-1.8	0.5-2.3	0.1-0.3	2.0-4.4
SAR	0.4-1.4	0.9-1.6	0.1-0.2	1.4-3.2
TOTAL	2.0-4.0	1.7-6.0	0.3-0.7	4.0-10.7

Table 2: Published local annually averaged estimates of $\overline{FCO_2}$ in mol C m^{-2} yr^{-1} for estuaries along the East coast of the US.**"**

Name	Lon	Lat	$\overline{FCO_2}$		Reference
			Observed.	Modeled	
Altamaha Sound	-81.3	31.3	32.4	72.7	Jiang et al. (2008)
Bellamy	-70.9	43.2	3.6	3.9	Hunt et al. (2010)
Cocheco	-70.9	43.2	3.1	3.9	Hunt et al. (2010)
Doboy Sound	-81.3	31.4	13.9	25.7	Jiang et al. (2008)
Great Bay	-70.9	43.1	3.6	3.9	Hunt et al. (2011)
Little Bay	-70.9	43.1	2.4	3.9	Hunt et al. (2011)
Oyster Bay	-70.9	43.1	4	3.9	Hunt et al. (2011)
Parker River estuary	-70.8	42.8	1.1	3.9	Raymond and Hopkinson (2003)
Sapelo Sound	-81.3	31.6	13.5	20.6	Jiang et al. (2008)
Satilla River	-81.5	31	42.5	25.7	Cai and Wang (1998)
York River	-76.4	37.2	6.2	8.1	Raymond et al. (2000)
Hudson River	-74	40.6	13.5	15.5	Raymond et al. (1997)

1304 **Table 3:** State variables and processes explicitly implemented in CGEM.

State variables		
Name	**Symbol**	**Unit**
Suspended Particulate Mater	SPM	gL^{-1}
Total Organic Carbon	TOC	µM C
Nitrate	NO_3	µM N
Ammonium	NH_4	µM N
Phosphate	DIP	µM P
Dissolved Oxygen	DO	µM O_2
Phytoplankton	Phy	µM C
Dissolved Silica	dSi	µM Si
Dissolved Inorganic Carbon	DIC	µM C
Biogeochemical reactions		
Name	**Symbol**	**Unit**
Gross primary production	GPP	µM C s^{-1}
Net primary production	NPP	µM C s^{-1}
Phytoplankton mortality	M	µM C s^{-1}
Aerobic degradation	R	µM C s^{-1}
Denitrification	D	µM C s^{-1}
Nitrification	N	µM N s^{-1}
O_2 exchange with the atmosphere	FO_2	µM O_2 s^{-1}
CO_2 exchange with the atmosphere	FCO_2	µM C s^{-1}
SPM erosion	E_{SPM}	gL^{-1} s^{-1}
SPM deposition	D_{SPM}	gL^{-1} s^{-1}

1305

1306

Table 4: Yearly averaged surface area (*S*), fresh water discharge (*Q*), residence time (*Rt*), FCO_2 and *NEM* of all simulated estuaries.

long *degrees*	lat *degrees*	*S* km^2	*Q* $m^3 s^{-1}$	*Rt* *days*	$\overline{FCO_2}$ *mol C* m^{-2} yr^{-1}	$\overline{NEM}$ *mol C* m^{-2} yr^{-1}	FCO_2 10^6 *mol C* yr^{-1}	*NEM* 10^6 *mol C* yr^{-1}
NAR								
-67.25	44.75	7	38.5	15	3.7	-37.4	27	-270
-67.25	45.25	12	73.6	15	6.0	-56.7	71	-666
-67.25	45.25	12	73.6	15	13.8	-56.6	162	-666
-67.75	44.75	3	68.5	4	6.7	-63.5	23	-221
-68.25	44.75	14	69.5	19	4.1	-56.2	58	-791
-68.75	44.75	89	309.9	23	27.4	-58.2	2431	-5163
-69.75	44.25	50	626.6	5	32.3	-74.4	1607	-3703
-70.25	43.75	3	25.8	10	2.1	-21.0	7	-71
-70.75	41.75	288	103.6	958	5.0	-4.0	1428	-1146
-70.75	42.25	63	210.7	40	16.2	-32.9	1025	-2081
-70.75	42.75	17	105.8	3	56.3	-69.0	943	-1155
MAR								
-70.75	43.25	31	29.9	11	21.6	-37.4	662	-1146
-71.25	41.75	257	28.2	808	3.9	-2.5	997	-650
-71.75	41.25	21	112.4	4	35.2	-32.6	726	-672
-72.75	40.75	20	25.4	62	30.7	-21.1	623	-430
-72.75	41.25	10	142.5	2	150.8	-36.9	1578	-386
-72.75	41.75	55	476.6	3	55.9	-45.7	3088	-2523
-73.25	40.75	19	26.8	56	31.4	-28.4	608	-550
-74.25	40.75	1192	608.2	126	15.5	-11.8	18432	-14047
-75.25	38.25	399	80.5	172	13.9	-5.0	5558	-2016
-75.25	38.75	354	31.8	357	7.5	-3.0	2659	-1076
-75.25	39.75	1716	499.0	221	10.0	-7.8	17072	-13439
-75.75	39.25	224	18.3	434	7.5	-2.9	1685	-640
-76.25	39.25	3427	717.1	352	8.1	-5.1	27646	-17352
-76.75	37.25	586	272.3	74	15.0	-10.4	8810	-6084
-76.75	37.75	154	36.3	163	10.7	-6.6	1654	-1023
-76.75	39.25	59	71.2	29	48.6	-34.6	2862	-2038
-77.25	38.25	206	30.2	268	6.1	-3.3	1265	-676
-77.25	38.75	568	259.2	118	16.7	-10.8	9488	-6134
SAR								
-78.25	34.25	48	167.4	7	122.5	-62.4	5916	-3015
-79.25	33.25	47	56.3	42	43.4	-36.5	2056	-1728
-79.25	33.75	45	291.4	8	85.1	-78.7	3843	-3551
-79.75	33.25	25	33.8	15	37.9	-32.8	956	-828
-80.25	32.75	25	31.0	50	48.8	-42.5	1214	-1057
-80.25	33.25	92	75.5	61	62.7	-61.2	5769	-5625
-80.75	32.25	71	21.1	182	12.9	-7.0	918	-501
-80.75	32.75	164	63.1	95	20.6	-11.5	3372	-1879
-81.25	31.75	92	71.7	45	25.7	-20.9	2361	-1926
-81.25	32.25	130	379.8	11	51.7	-39.2	6732	-5097
-81.75	30.75	34	18.7	61	17.5	-14.7	602	-505
-81.75	31.25	130	17.7	294	5.5	-4.0	713	-523
-81.75	31.75	56	350.5	4	72.7	-67.4	4068	-3770

Table 5: Seasonal contribution to FCO_2 and *NEM* in each the sub-region. The seasons displaying the highest percentages are indicated in bold. Winter is defined as January, February and March, Spring as April, May and June and so on…

Region	*S*	*NEM*	winter	spring	summer	fall	FCO_2	winter	spring	summer	fall
	km^2	mol C y^{-1}	%	%	%	%	mol C y^{-1}	%	%	%	%
NAR	558	-16.3 10^9	14.7	21.2	**37.0**	27.2	7.2 10^9	26.3	18.9	26.5	**28.3**
MAR	9298	-72.2 10^9	21.9	25.9	**28.8**	23.4	108.3 10^9	**29.8**	23.3	20.7	26.2
SAR	959	-30.5 10^9	24.6	20.9	**30.3**	24.2	39.2 10^9	26	23.4	**27**	23.6

1315 **Table 6:** Regressions and associated coefficient of determination between the depth normalized
1316 residence time (S/Q) and -$\overline{NEM}$ / *f(T)*, $\overline{FCO_2}$ / *f(T)* and *CFilt*.

Region	$-\overline{NEM}/f(T)$	$\overline{FCO_2}/f(T)$	*CFilt*
NAR	$y = 27.84\ x^{-0.17}$ $r^2 = 0.11$	$y = 6.07\ x^{0.00}$ $r^2 = 0.00$	$y = 15.08 \log_{10}(x) + 4.86$ $r^2 = 0.40$
MAR	$y = 26.03\ x^{-0.63}$ $r^2 = 0.86$	$y = 34.36\ x^{-0.58}$ $r^2 = 0.68$	$y = 40.46 \log_{10}(x) + 9.60$ $r^2 = 0.70$
SAR	$y = 28.36\ x^{-0.71}$ $r^2 = 0.76$	$y = 32.82\ x^{-0.66}$ $r^2 = 0.80$	$y = 23.19 \log_{10}(x) + 43.71$ $r^2 = 0.46$
MAR + SAR	$y = 25.85\ x^{-0.64}$ $r^2 = 0.82$	$y = 31.64\ x^{-0.58}$ $r^2 = 0.70$	$y = 33.30 \log_{10}(x) + 24.88$ $r^2 = 0.57$
NAR + MAR + SAR	$y = 28.98\ x^{-0.66}$ $r^2 = 0.82$	$y = 12.98\ x^{-0.33}$ $r^2 = 0.30$	$y = 40.64 \log_{10}(x) + 11.84$ $r^2 = 0.70$

1317

1318

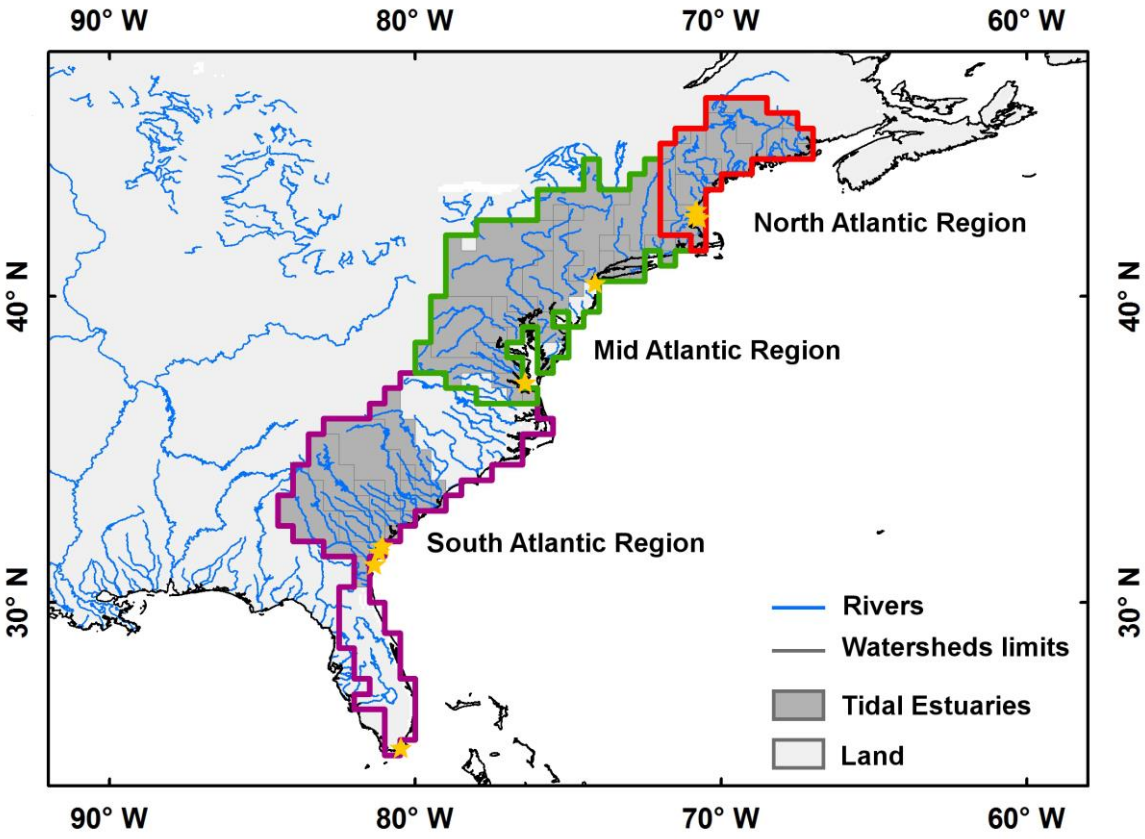

1319

1320 **Figure 1**: Limits of the 0.5 degrees resolution watersheds corresponding to tidal estuaries of the East
1321 coast of the US. 3 sub-regions are delimited with colors and orange stars represent the location of
1322 previous studies.

1323

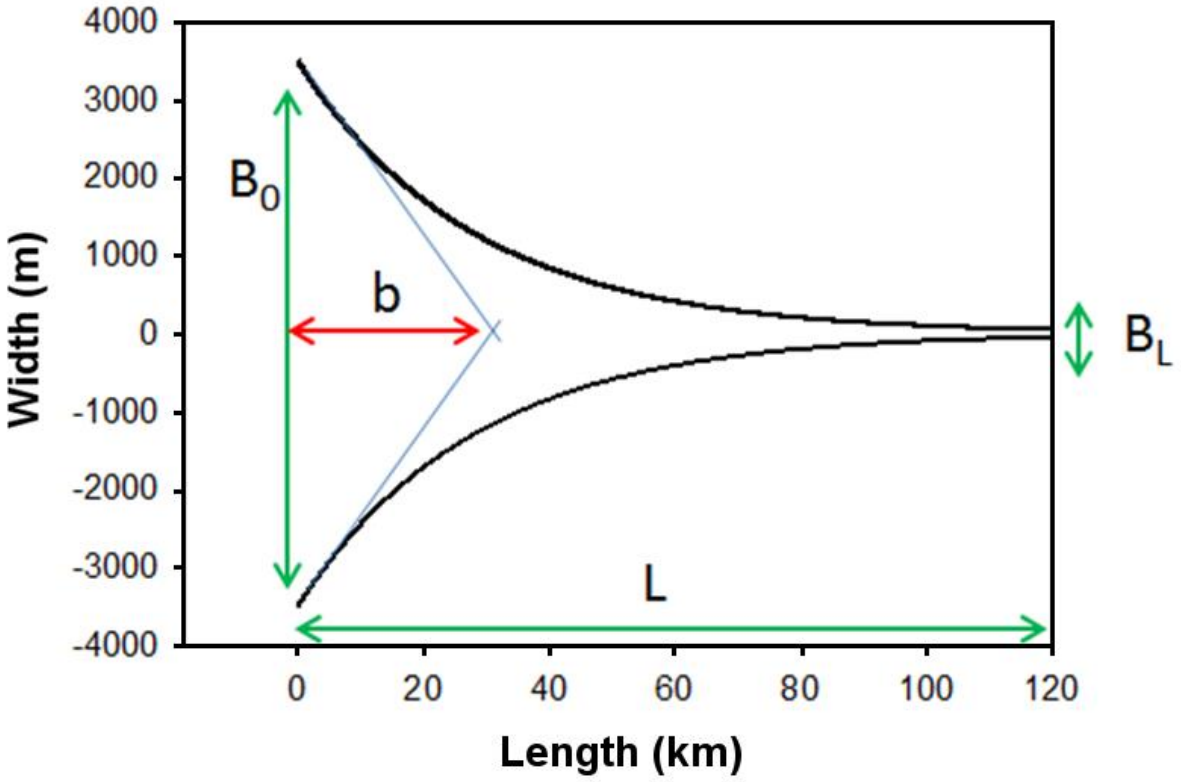

Figure 2: Idealized estuarine geometry and main parameters. Parameters indicated by green arrows are measured, b is calculated. See section 2.3.1 for further details.

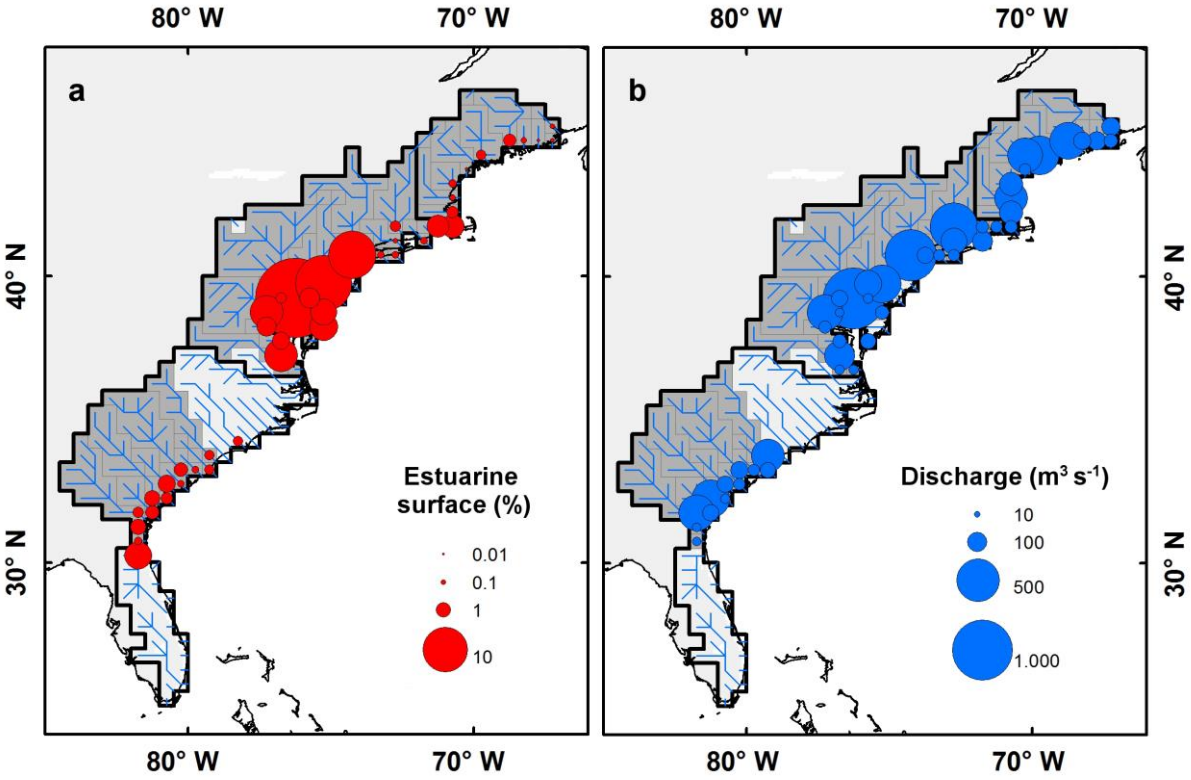

Figure 3: Estuarine surface area (a) and mean annual freshwater discharge (b) for each tidal estuary of the East coast of the US. Estuarine surface area are expressed as percentage of the entire surface area of the region (19830 km^2)

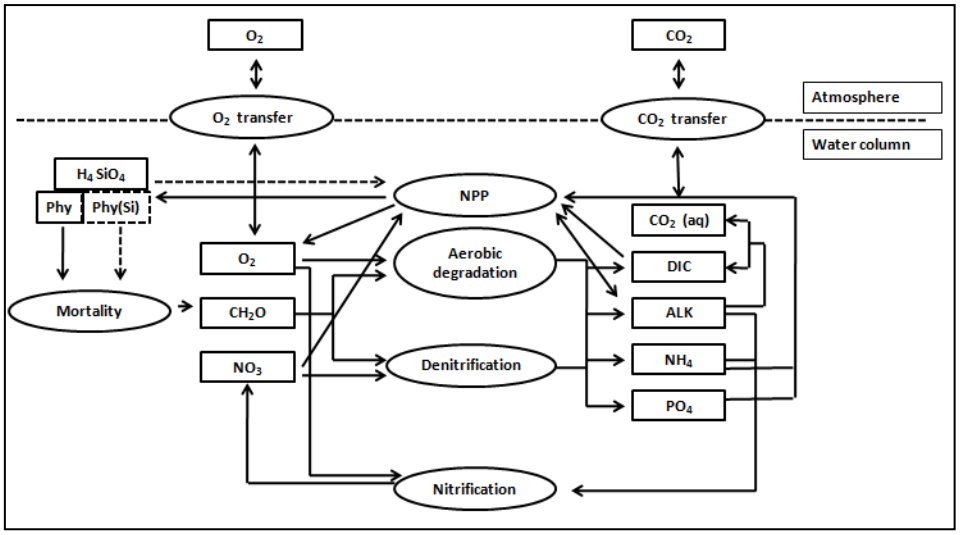

1334

1335 **Figure 4:** Conceptual scheme of the biogeochemical module of C-GEM used in this study. State-
1336 variables and processes are represented by boxes and oval shapes, respectively. Modified from Volta
1337 et al., 2014.

1338

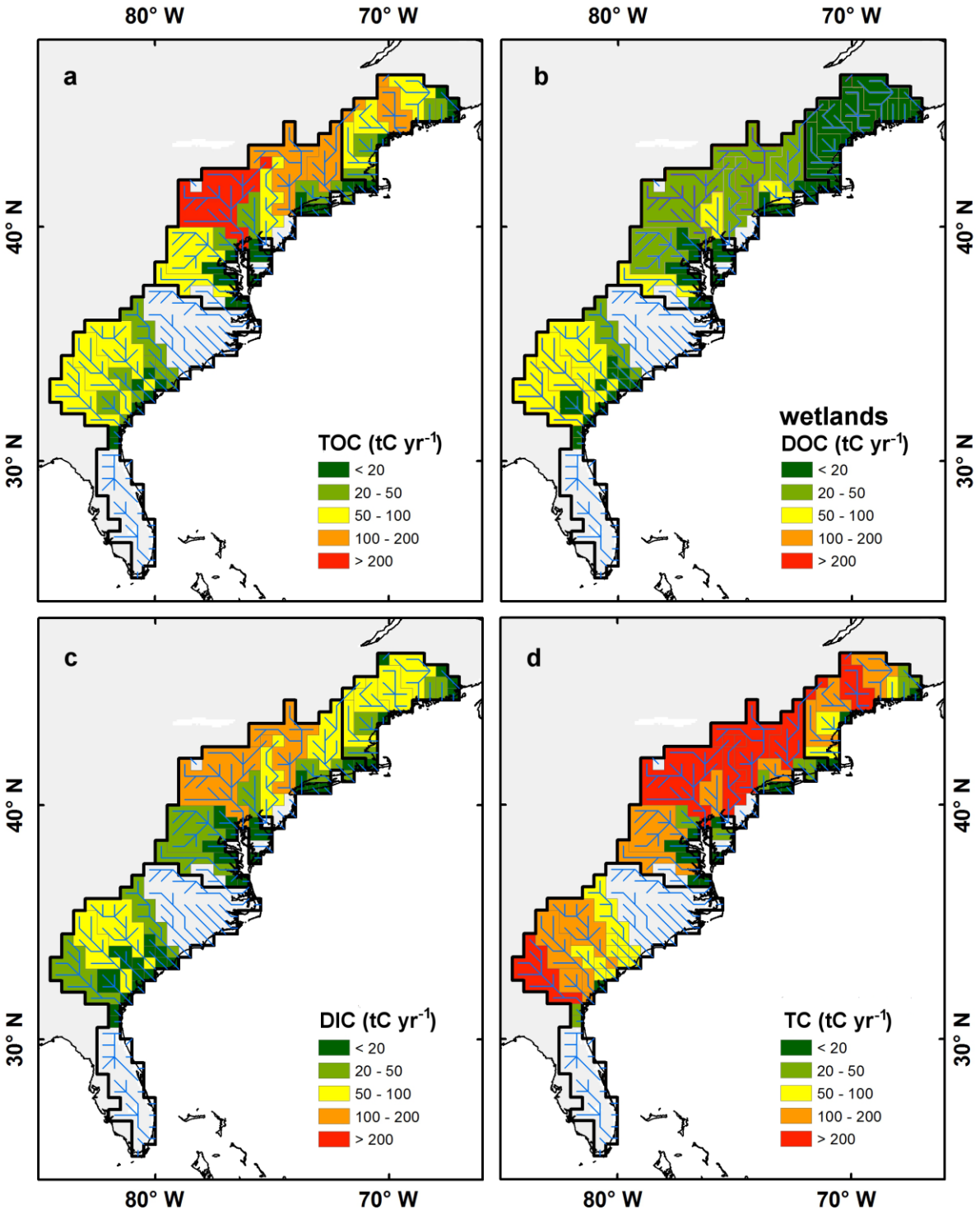

1339

1340 **Figure 5:** Annual river carbon loads of TOC (a), annual DOC fluxes from wetlands (b), annual river
1341 carbon loads of DIC (c) and annual TC fluxes (d). All fluxes are indicated per watershed.

1342

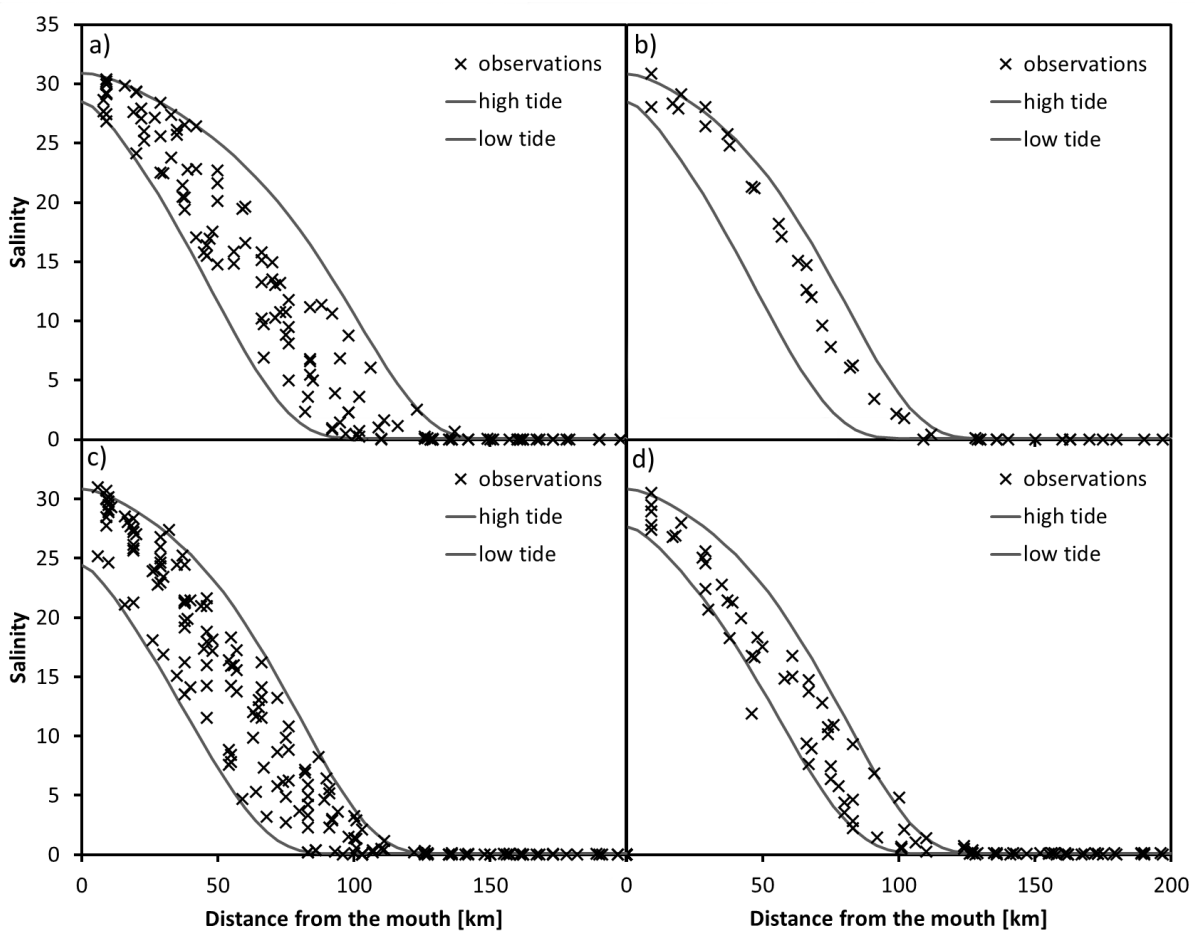

1343

1344 **Figure 6.** Modeled (lines) and measured (crosses) salinities in the Delaware Bay estuary for January

1345 (a), February (b), May (c), June (d). The two lines correspond to high and low tides.

1346

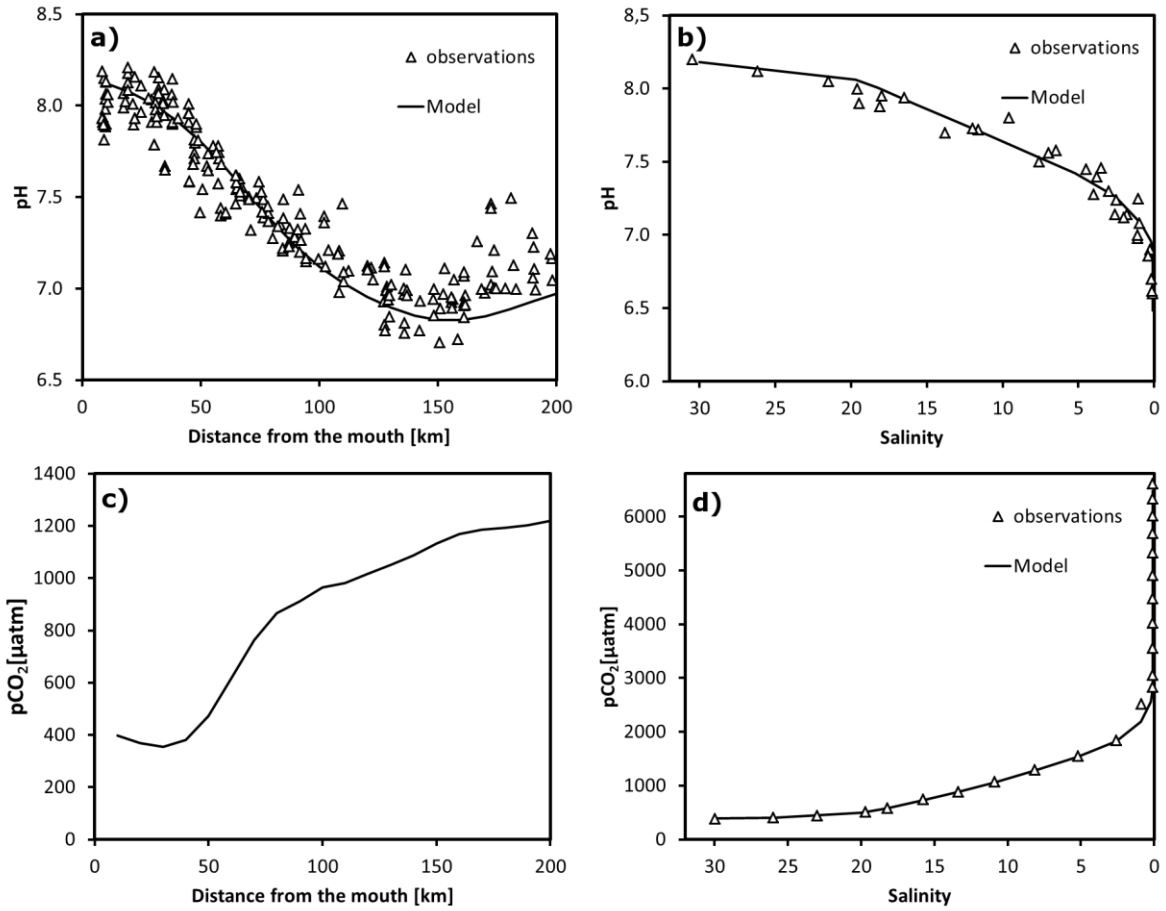

1347

1348 **Figure 7.** Longitudinal profiles of pH (top) and pCO_2 (bottom) for the Delaware Bay (left) and
1349 Altamaha river estuary (right).

1350

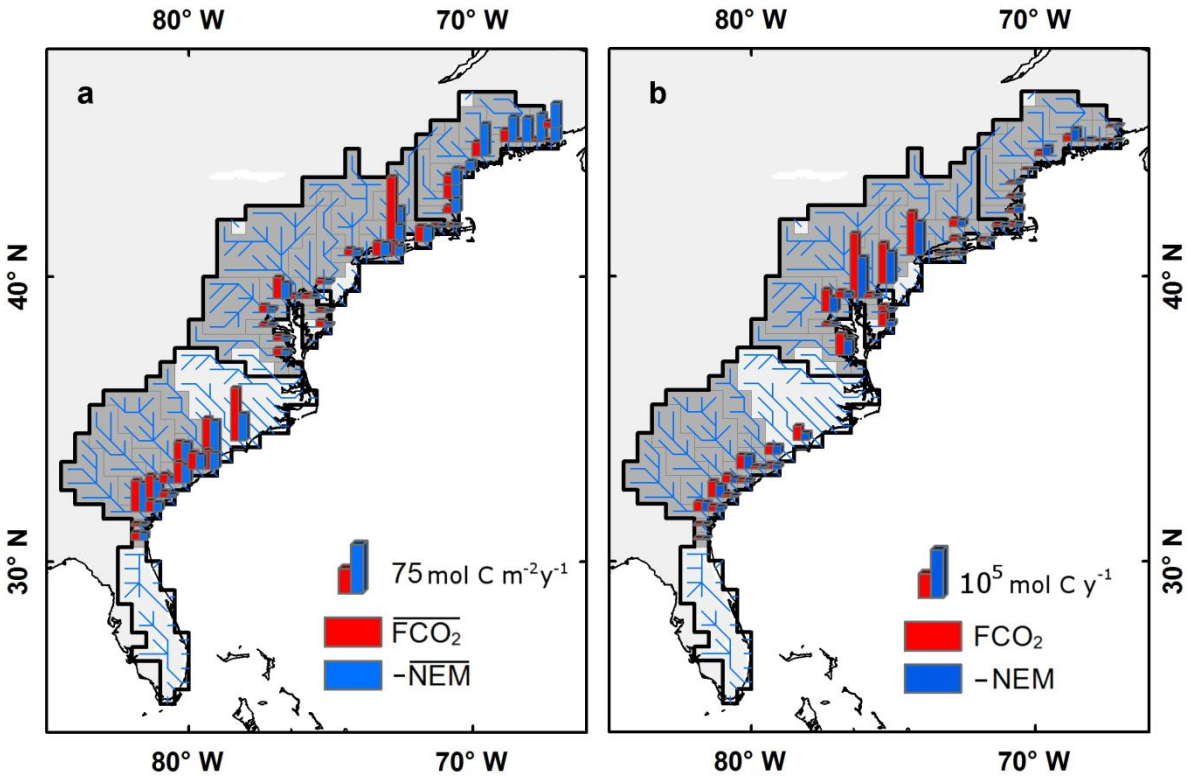

Figure 8: Spatial distribution of spatially averaged value (a) and integrated value (b) of mean annual FCO_2 (red) and -*NEM* (blue) along the East coast of the US. On panel a, the notation with overbars ($\overline{FCO_2}$ and -$\overline{NEM}$) represents rates per unit surface. For the sake of the comparison with $\overline{FCO_2}$, Fig. 8 displays -$\overline{NEM}$ because the model predicts that all estuaries in this region are net heterotrophic.

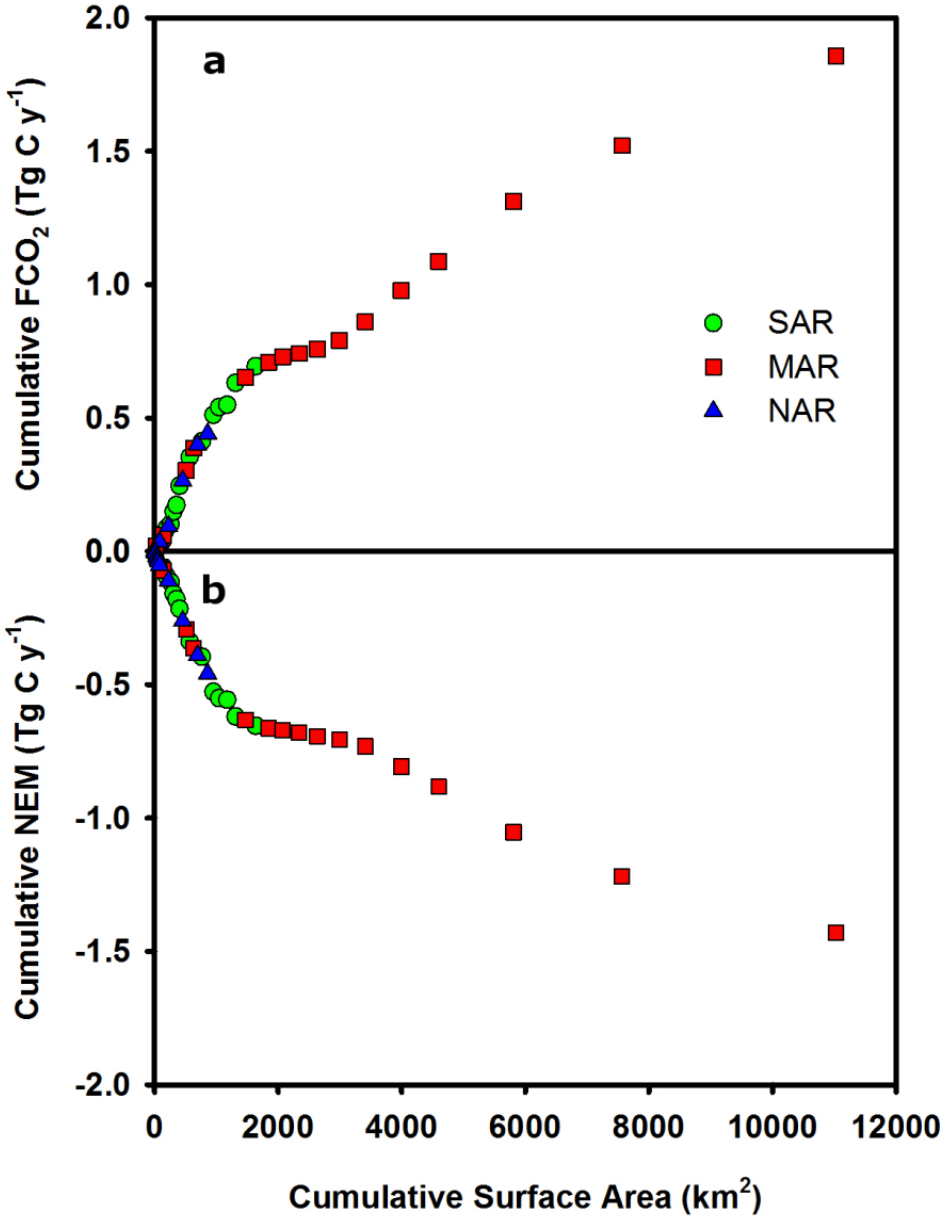

1358

1359 **Figure 9:** The Cumulative *FCO_2* (a) and *NEM* (b) as functions of the cumulative estuarine surface area.
1360 Systems are sorted by increasing surface area.

1361

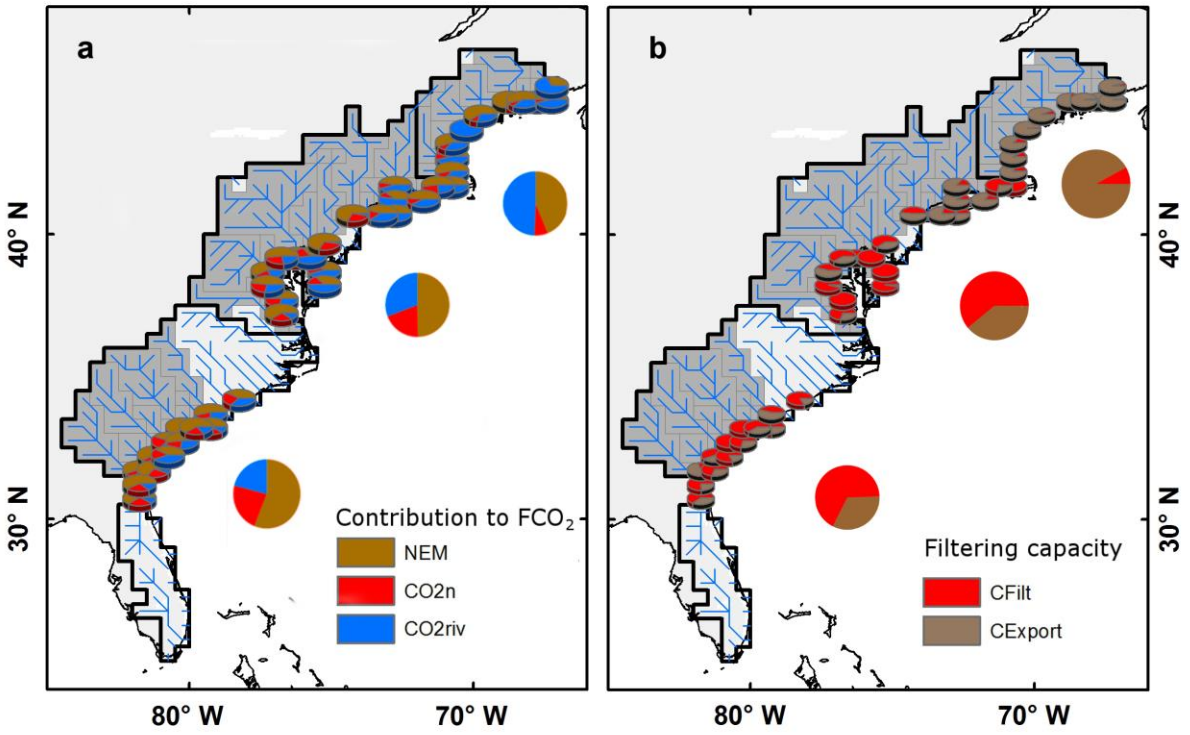

Figure 10: Contribution of *NEM*, nitrification and riverine waters super-saturated waters to the mean annual FCO_2 (a). Spatial distribution of mean annual carbon filtration capacities (*CFilt*) and export (*CExport*) along the East coast of the US (b).

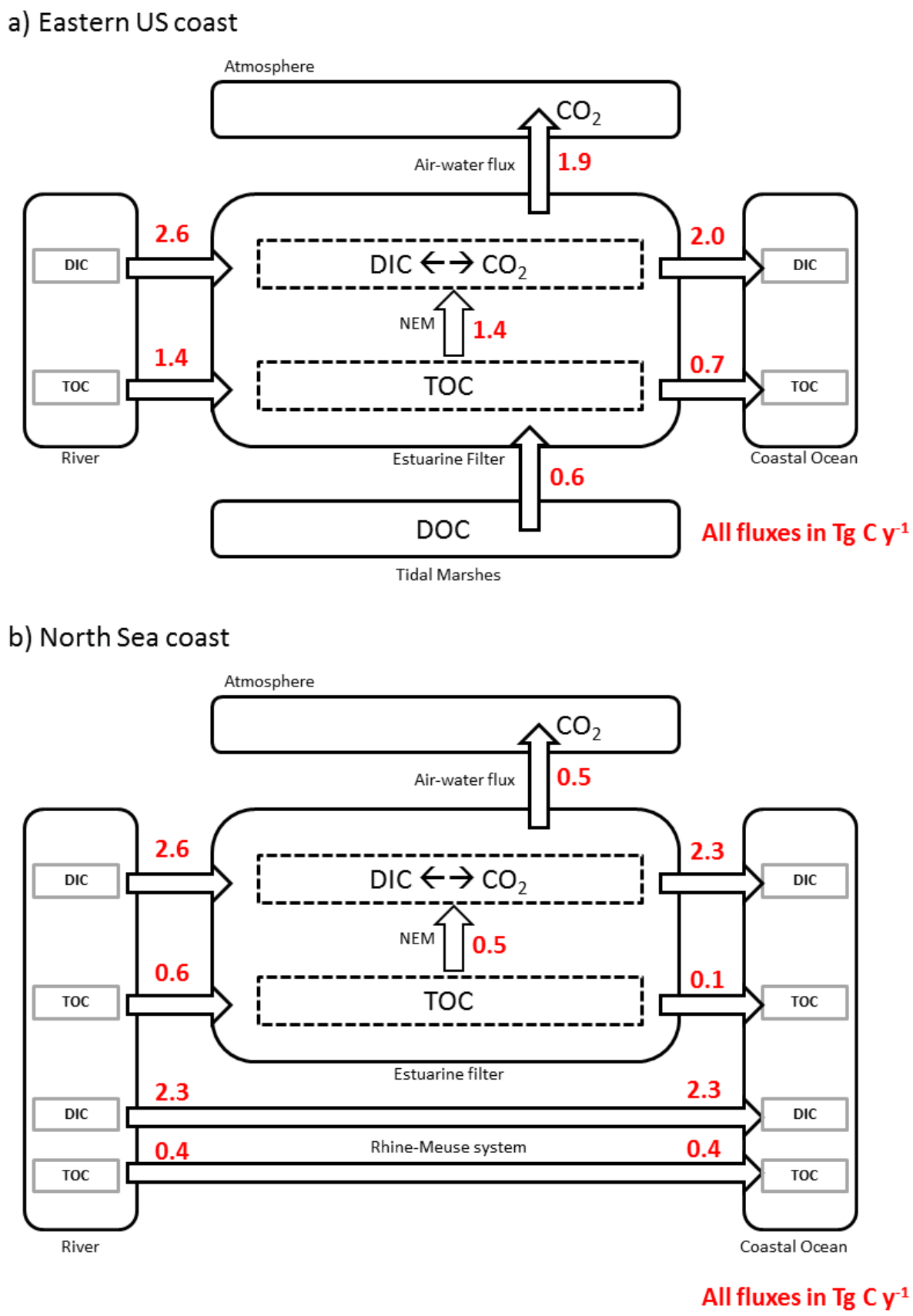

1367

1368 **Figure 11:** Annual carbon budget of the estuaries of the East coast of the US (a) and of the coast of
1369 the North Sea (b, modified from Volta et al., 2016a).

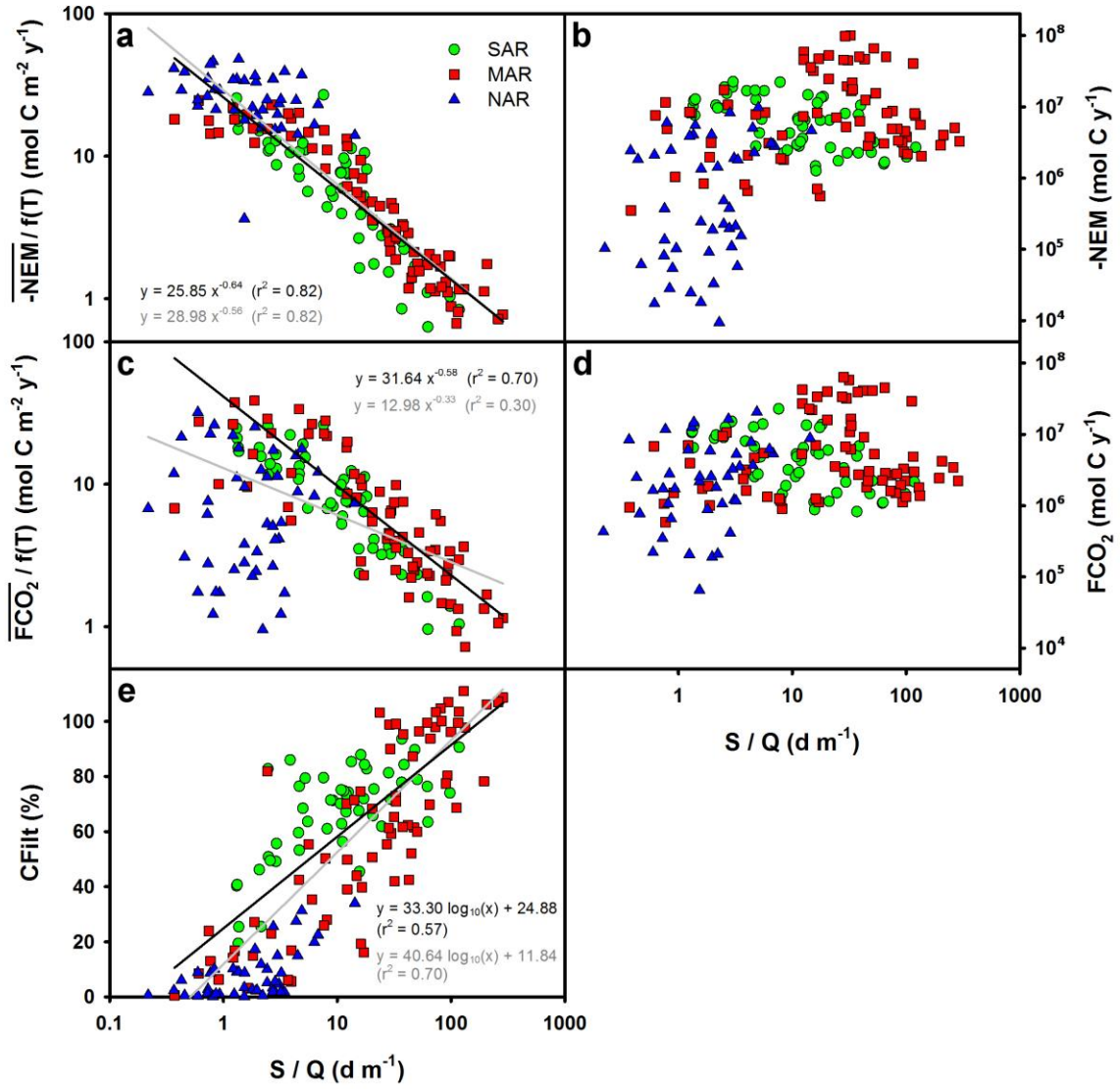

1370

1371 **Figure 12:** System scale integrated biogeochemical indicators expressed as functions of the depth
1372 normalized residence time expressed as the ratio of the estuarine surface S and the river discharge Q
1373 for all seasons. Panels b, d and e represent -NEM, FCO_2 and CFilt, respectively. Panels a and c
1374 represent -NEM, FCO_2 normalized by a temperature Q_{10} function. Black lines are the best fitted linear
1375 regressions obtained using all the point. Grey lines are best fit using only the estuaries from the MAR
1376 and SAR regions.

1377